NMR and Molecular Dynamics Studies of the Conformational Epitope of the Type III Group B *Streptococcus* Capsular Polysaccharide and Derivatives[†]

Jean-Robert Brisson,[‡] Stanislava Uhrinova,[‡] Robert J. Woods,[‡,§] Mark van der Zwan,[‡] Harold C. Jarrell,[‡] Lawrence C. Paoletti,[||] Dennis L. Kasper,[||] and Harold J. Jennings*[,‡]

Institute for Biological Sciences, National Research Council of Canada, Ottawa, Canada K1A 0R6, and Channing Laboratory, Harvard Medical School, Boston, Massachusetts 02115

Received July 23, 1996; Revised Manuscript Received December 3, 1996[⊗]

ABSTRACT: The conformational epitope of the type III group B *Streptococcus* capsular polysaccharide (GBSP III) exhibits unique properties which can be ascribed to the presence of sialic acid in its structure and the requirement for an extended binding site. By means of NMR and molecular dynamics studies on GBSP III and its fragments, the extended epitope of GBSP III was further defined. The influence of sialic acid on the conformational properties of GBSP III was examined by performing conformational analysis on desialylated GBSP III, which is identical to the polysaccharide of *Streptococcus pneumoniae* type 14, and also on oxidized and reduced GBSP III. Conformational changes were gauged by ^{1}H and ^{13}C chemical shift analysis, NOE, 1D selective TOCSY−NOESY experiments, J_{HH} and J_{CH} variations, and NOE of OH resonances. Changes in mobility were examined by ^{13}C T_1 and T_2 measurements. Unrestrained molecular dynamics simulations with explicit water using the AMBER force field and the GLYCAM parameter set were used to assess static and dynamic conformational models, simulate the observable NMR parameters and calculate helical parameters. GBSP III was found to be capable of forming extended helices. Hence, the length dependence of the conformational epitope could be explained by its location on extended helices within the random coil structure of GBSP III. The interaction of sialic acid with the backbone of the PS was also found to be important in defining the conformational epitope of GBSP III.

Group B *Streptococcus* is a major cause of neonatal sepsis and meningitis (Baker & Edwards, 1988). Group B streptococci are Gram-positive organisms which have been classified on the basis of their different type-specific polysaccharides into types Ia, Ib, and II−VIII (Kogan et al., 1996; Ferrieri, 1990). The structures of the repeating units of all the above polysaccharides have been determined (Kogan et al., 1994, 1995; Wessels et al., 1991; DiFabio et al., 1989; Jennings, 1990), and the strains most commonly isolated from clinical cases belong to types Ia, Ib, II, and III (Baker & Kasper, 1985). The structures of the group B streptococcal polysaccharides are unique firstly because they have such close structural similarities. All of them contain terminal sialic acid and even more extensive sequence homology. Secondly, they exhibit extensive structural homology with oligosaccharide components of human tissue antigens (Jennings et al., 1984). Despite their close structural similarities, all the polysaccharides also exhibit a high degree of immunological specificity. This together with other evidence demonstrates that terminal sialic acid is not immunodominant (Jennings et al., 1984). However, despite this, it has been shown to be essential to the formation of GBSP III[1] specific antibodies. Thus, it was proposed that sialic acid, through its interaction with the backbone of GBSP III, exerts conformational control over the epitope responsible for the above antibodies. It was further established that while the carboxylate groups of the terminal sialic acid residues are essential to the formation of this epitope, other structural features of sialic acid are not (Jennings et al., 1981).

Extensive studies on the immunological properties of GBSP III have further defined this epitope. Using fragments of the GBSP III it was ascertained that the epitope had an unusual length dependency, requiring at least a decasaccharide for suboptimal binding (Wessels et al., 1987b) and in addition that the affinity of binding increased with increasing chain length (Wessels et al., 1987a). These properties can be rationalized in terms of the presence of a conformational epitope situated on an extended segment of the GBSP III. Similar chain length-dependent conformational epitopes have been described for the polysaccharides of group B *Neisseria meningitidis* (Jennings et al., 1985) and *Streptococcus pneumoniae* type 14 (Wessels & Kasper, 1989) and, in the case of the former, evidence was obtained for the epitope

[†] This is National Research Council of Canada Publication 39539. This work was supported by NIAID grant R37AI23339 and NIAID contract AI25152.

* To whom correspondence should be addressed.

[‡] National Research Council of Canada.

[§] Present address: Complex Carbohydrate Research Center, The University of Georgia, Athens, GA 30602-4712.

[||] Harvard Medical School.

[⊗] Abstract published in *Advance ACS Abstracts,* February 15, 1997.

[1] Abbreviations: 1D, one dimensional; 2D, two-dimensional; COSY, correlation spectroscopy; CPS, capsular polysaccharide; DANTE, delays with alternating nutations for tailored excitation; Gal, galactose; Glc, glucose; GlcNAc, *N*-acetyl-glucosamine; GBS III, type III group B *Streptococcus*; GBSP III, type III group B *Streptococcus* capsular polysaccharide; HMQC, heteronuclear multiple quantum coherence; HSQC, heteronuclear single quantum coherence; OS, oligosaccharide; NeuAc, *N*-acetyl neuraminic acid, sialic acid; NOE, nuclear Overhauser enhancements; NOESY, NOE correlated spectroscopy; PS, polysaccharide; TOCSY, total correlation spectroscopy; TPPI, time-proportional phase increment.

S0006-2960(96)01819-3 CCC: $14.00 © 1997 American Chemical Society

being situated on an extended helical segment of the polysaccharide (Evans et al., 1995).

By means of NMR studies and molecular dynamics simulations on GBSP III and its fragments, this paper attempts to further define the conformational properties of the GBSP III extended epitope in order to understand its immunological properties. The influence of sialic acid on the conformational properties of GBSP III was examined by performing conformational analysis on the desialylated GBSP III which is identical to the polysaccharide of *S. pneumoniae* type 14 and also on oxidized and reduced GBSP III.

EXPERIMENTAL PROCEDURES

NMR Methods. GBSP III (Wessels et al., 1987b) and desialylated GBSP III (Wessels & Kasper, 1989) were enzymatically hydrolyzed by an endo-β-galactosidase into oligosaccharide fragments of one or more pentasaccharide repeating units which were isolated and purified (Paoletti & Johnson, 1995). The reduced and oxidized GBSP III were obtained by standard chemical procedures (Jennings et al., 1981). The structures of all the products of the above reactions were confirmed by ^{1}H NMR. Replacement of the sodium cation by the tetramethylammonium cation was obtained by dialysis. The compounds (3−6 mg each), previously lyophilized and dried under high vacuum, were dissolved in 0.5 mL of 99.96% D_2O, bubbled with nitrogen for 15 min, and sealed in NMR tubes. The pH value of the solutions of sialo compounds was set prior the lyophilization to pH 7.0 ± 0.1. The NMR experiments were performed on a Bruker AMX-600 spectrometer. The ^{1}H spectra and ^{13}C spectra were referenced to acetone by setting the methyl signal to 2.225 ppm in ^{1}H spectra and 31.07 ppm in ^{13}C spectra. Most of the experiments were performed at 290 K.

For the measurement of the hydroxyl resonances experiments were performed in 65% H_2O, 35% $(CD_3)_2CO$ at 260−280 K. The spectra were acquired using the 1−1 spin−echo experiment further implemented in the 2D TOCSY and 2D NOESY (Bax et al., 1987; Sklenar & Bax, 1987). NOE interactions in the sialopentasaccharide were studied by 1D NOE difference spectroscopy using the 1−1 spin−echo sequence as a reading pulse, the interval between the pulses was 400 μs, and the saturation time for each hydroxyl proton was 0.7 s. The relaxation delay was 1.5 s, the acquisition time was 0.5 s with 2048 scans. The intensity of the solvent signal was reduced by Gaussian convolution (Marion et al., 1989) using the Felix processing program.

Assignments of the ^{1}H spectra were obtained from a 2D TOCSY experiment (Bax & Davis, 1985) with mixing times from 40 to 90 ms. 2D triple quantum filtered COSY (Shaka & Freeman, 1983) was used to detect the three-spin systems in the one and two repeat units. Vicinal coupling constants were extracted by 1D TOCSY and 1D NOESY (Kessler et al., 1989). The selective excitation was achieved by a half-Gaussian pulse. The transfer step in 1D TOCSY was adjusted from 12 to 60 ms. The mixing time for NOE transfer was 300 ms. The population for different rotational states of pendant-CH_2OH groups were estimated both on the basis of NOE contacts between the ring protons and from vicinal coupling constants by using Karplus type equations for CH_2OH groups (Haasnoot et al., 1980).

2D NOESY spectra were measured in the TPPI mode (Bodenhausen et al., 1984). Spectra were recorded at 290 K (280 K for $[c(ed)ba]_1$), with 512 t_1 increments, the number of transitions varied from 32 to 64 scans, and a spectral width of 2400 Hz (4 ppm) was zero-filled to a 2048 × 1024 matrix. All the 2D spectra were weighted with the squared sine bell function shifted by $\pi/2$ in both dimensions with appropriate baseline correction. The NOE buildup curves for $[c(ed)ba]_1$ were obtained with mixing times from 75 to 1000 ms and a recycle delay of 2.4 s. Peak volumes were measured by standard Bruker 2D integration routine. The NOEs of sialic acid and several overlapping spins were analyzed by 1D selective TOCSY−NOESY experiment (Uhrin et al., 1994). In the TOCSY step, a 90° half Gaussian shaped pulse was used, and the mixing time was optimized for appropriate transfer of magnetization. The 180° selective pulse in the NOESY step was produced by DANTE Z pulse train (10 ms); the delay for NOE varied with the size of the compounds from 50 to 300 ms.

The ^{13}C signals of selected oligosaccharides were further analyzed by 2D HMQC (Bax et al., 1983) and 2D HMQC−TOCSY (Lerner & Bax, 1986). A 2D HSQC experiment (Bodenhausen & Ruben, 1980) with presaturation of water was used to reveal one-bond $^1J_{CH}$ connectivities. The $^3J_{CH}$ coupling constants across the glycosidic linkage were measured by 2D experiments with inverse detection and suppression of ^1J modulation (Uhrin et al., 1992) and were determined within an accuracy of ±0.1 Hz by substraction of the inphase multiplets obtained by 1D selective methods (Uhrin et al., 1996).

Relaxation Measurements and Analysis. The ^{13}C T_1 and T_2 measurements were performed by double-INEPT type inverse-detected experiments with suppression of cross-correlation and cross-relaxation (Boyd et al., 1990; Kay et al., 1992; Szyperski et al., 1993). The integral intensities of the signals from six to eight measurements were fitted to the exponential decay, $I = I_o \exp(\tau/T)$, where τ is evolution time and T corresponds to T_1 or T_2 ^{13}C-relaxation time. The ^{13}C-relaxation data were analyzed using a model-free approach (Lipari & Szabo, 1982a). It was assumed that relaxation was purely through the ^{1}H−^{13}C mechanism so that the spin-lattice relaxation rate and transverse relaxation rate for a protonated carbon are given by

$$\frac{1}{T_1} = \frac{\gamma_C^2 \gamma_H^2 \hbar^2}{4 r_{CH}^6}[J(\omega_H - \omega_C) + 3J(\omega_C) + 6J(\omega_H + \omega_C)] \quad (1)$$

$$\frac{1}{T_2} = \frac{\gamma_H^2 \gamma_C^2 \hbar^2}{8 r_{CH}^6}[4J(0) + J(\omega_H - \omega_C) + J(\omega_C) + 6J(\omega_H) + 6J(\omega_H + \omega_C)] \quad (2)$$

where r_{CH} is taken to be 1.1 Å, $\hbar$ is Planck's constant, ω_H and ω_C are the Larmor frequencies in rad s^{-1}, and γ_H and γ_C are the magnetogyric ratio for a proton and carbon, respectively.

Within the framework of the model-free analysis the spectral density function describing both internal and global motions is given for potentially anisotropic overall motion by

$$J(\omega) = \frac{2}{5}\left[S^2\left\{\frac{A\tau_1}{1+\omega^2{\tau_1}^2} + \frac{(1-A)\tau_2}{1+\omega^2{\tau_2}^2}\right\} + (1-S^2)\left\{\frac{A\tau_{1e}}{1+\omega^2{\tau_{1e}}^2} + \frac{(1-A)\tau_{2e}}{1+\omega^2{\tau_{2e}}^2}\right\}\right] \quad (3)$$

with $1/\tau_{1e} = 1/\tau_1 + 1/\tau_i$ and $1/\tau_{2e} = 1/\tau_2 + 1/\tau_i$, where τ_1 and τ_2 represent the two correlation times describing the overall reorientation of the molecule and A is a mixing coefficient which ranges from a value of 0 to 1. In the case of isotropic overall reorientation $\tau_1 = \tau_2$ and eq 3 simplifies to that given by Lipari and Szabo (1982a) for isotropic overall motion). The generalized order parameter S describes the spatial restriction of the internal motions which have an effective correlation time τ_i.

In the present study no assumption was made as to the nature of the overall reorientation or to the rate of motion (i.e., extreme narrowing was not assumed). Thus, the anisotropic form of the spectral density function depends on three global parameters, A ($0 \leq A < 1$), τ_1, and τ_2, and two local parameters, S ($0 \leq S < 1$) and τ_i, for each position. Measurement of T_1 and T_2 values allowed the data to be fit using eqs 1 and 2 and the global and local motional parameters extracted. In practice the data are fitted to an error function

$$error = \sum_{\omega_1}^{\omega_n}\sum_{i=1}^{N}\left[\frac{T_1^{obs} - T_1^{calc}}{T_1^{obs}}\right]_i^2 + \left[\frac{T_2^{obs} - T_2^{calc}}{T_1^{obs}}\right]_i^2 \quad (4)$$

which represents the difference between the observed and calculated values (Lipari & Szabo, 1982b; Palmer et al., 1991). This corresponds to a global minimization problem, and approaches to its solution for the model-free analysis have been described previously. In these approaches an estimate of the global parameters was required prior to fitting the local motional parameters. The present study used a different scheme to find the best solution to eqs 1 and 2 which is efficient at avoiding local minima and reaching a global minimum (or a local one that is almost as good as the true global minimum). The approach uses a modification (Press & Teukolsky 1991) which combines simulated annealing with downhill simplex minimization (Press et al., 1989). The minimization is started with initial arbitrary guesses as to the values of the three global and two local motional parameters, with the same values being used for each protonated carbon. The only constraints are that $t_i < t_1 < t_2$, $0 \leq S \leq 1$, and $0 \leq A \leq 1$. All $2N + 3$ parameters are adjusted simultaneously to give the lowest error. The "goodness" of the global minimum may be tested by doing a number of minimizations starting with substantially different initial values which are chosen using a random number generation routine. With test cases involving simulated relaxation data for 10 positions ($N = 10$), this routine was able to reproduce the "true" motional parameters starting with a number of different starting guesses. In the present study 20 fits were performed for each set of experimental data. A mean value and standard deviation (RMSD) for the global and local motional parameters were calculated from those fits for which the error in the fitting was 1.2 times the smallest error (best fit). Thus, a small RMSD reflects that the fitting procedure was not sensitive to the initial guesses used for the motional parameters and thus most likely represents the "true best fit".

Molecular Modeling. Minimizations and molecular dynamics (MD) simulations were performed with the MINMD or SANDER module of AMBER 4.0 (Pearlman et al., 1991), respectively, employing the GLYCAM_93 parameter set (Woods et al., 1995) extended for sialic acids, oligosaccharides, and glycoproteins on a DEC Alpha AXP 3000/800 computer. All atoms were treated explicitly. The initial oligosaccharide conformations were generated using the GLYCAM_93 monosaccharide structural data base and the LINK module of AMBER. In the case of anionic sugars, a sodium counterion was placed initially along the bisector of the carboxylate O−C−O angle a distance of 3 Å from the oxygen atoms. Periodic boundary conditions were employed, with TIP3P water molecules, and box dimensions were sufficient to allow for the faces of the box to extend 12 Å beyond the sugar in each direction. Typical box sizes ranged from 38.5 Å × 36.5 Å × 26.9 Å (1065 water molecules) for $[c(d)ba]_1$ to 63.6 Å × 41.6 Å × 41.4 Å (3270 waters) for $[c(ed)ba]_1$. The relatively large box size was chosen to enable the sugar to adopt highly extended conformations without introducing solute−solute interactions. All minimizations and subsequent dynamics were performed with a dielectric constant of unity. Cutoff values for nonbonded pair interactions of 10.0 and 8.0 Å were employed for anionic and neutral sugars, respectively. The initial water (and counterion, where present) configurations were subjected to 500 cycles of steepest descent energy minimization, during which the conformation of the sugar was frozen. Following this minimization, and in the case of anionic sugars only, a 50 ps MD simulation was performed, in which only the water molecules were allowed to move. This pre-equilibration was essential in order to avoid introducing artificially high velocities of the sodium counterion, arising from nonoptimal interactions between the ion and the water. Following the solvent pre-equilibration in the ionic systems, the water configurations were subjected to 500 cycles of steepest descent energy minimization, while both the sugar and counterion were frozen. Subsequently, for both ionic and neutral systems, all the atoms were subjected to 500 cycles of steepest descent minimization. The migration of the sodium ion is noteworthy. These initial configurations were then heated to 300 K over a period of 100 ps. During the MD simulations a constant temperature of 300 K was maintained through weak coupling to an external bath with a solvent coupling constant (TAUTS) of 0.25 ps^{-1} and a solute coupling constant (TAUTP) of 0.25 ps^{-1}. All hydrogen-containing bond lengths were constrained to their equilibrium values through application of the SHAKE algorithm. Newton's equations of motion were integrated using a Verlet algorithm with a 2 fs time step. Initial atomic velocities were assigned from a Maxwellian distribution at 5 K. During the dynamics a constant pressure of 1 atm was maintained with isotropic position scaling and a pressure relaxation time (TAUP) of 0.2 ps^{-1}. All 1−4 nonbonded interactions were scaled (SCNB) by the standard value of 2.0, whereas all 1−4 electrostatic interactions were scaled (SCEE) by a value of 1.2 as recommended recently for polyhydroxylated molecules (Cornell et al., 1993). The dynamics simulations were not in any way constrained to reproduce observable parameters, such as NOE or J coupling constants.

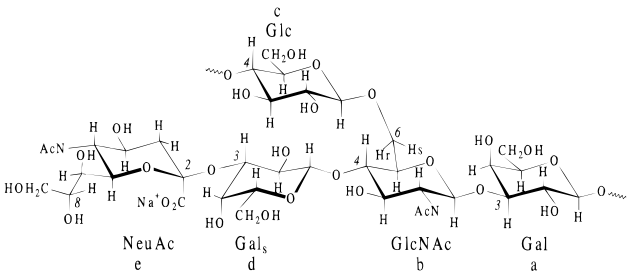

FIGURE 1: Structure and nomenclature for the repeat unit of GBSP III denoted as [c(ed)ba]$_n$, where n denotes the number of repeat units. The desialylated repeat units which have the same structure of *S. pneumonia* type 14 are denoted by [c(d)ba]$_n$.

From the molecular dynamics trajectories the ensemble averaged NOE, the helical parameters, and $^3J_{CH}$ couplings constants were calculated as described before (Tvaroska et al., 1989; Brisson et al., 1992). The helical parameters were described using the polar (ρ, λ) representation of the (n, h) helical parameters, where n is the number of residues per turn of the helix and h is the translation along the helix axis of corresponding residues. The percentage of the maximum elongation is represented by $\lambda = h/L$, where L is the length of the virtual bond between two adjacent linking atoms and represents the maximum rise per turn or elongation of the helix. The parameter $\rho = 360°/n$ avoids the discontinuity when $n = 2$ or $h = 0$. The chirality of the helix was defined by the sign of ρ, with right-handed helices having ρ values from 0° to 180° and left-handed helices from 0° to −180°. The polar (ρ, λ) representation is used to compare at a glance the secondary structures displayed by various polysaccharides (Perez & Vergelati, 1985). Potential energy calculations using PFOS and calculations of the helical parameters as a function of the 1−6 linkage angles were done as described before (Brisson et al., 1992).

RESULTS

The conformation of native and desialylated polysaccharide and their related oligosaccharide fragments was investigated. The nomenclature used to denote the various fragments is given in Figure 1. The modified sialopolysaccharides with reduced and oxidized sialic acid residues and the tetramethylammonium salt solution were also examined. Both experimental and computational methods were used to define conformational models. Unrestrained molecular dynamics calculations with explicit water using the AMBER force field and the GLYCAM parameter set were used. The conformational analysis by NMR was based on the measurement of the NOE for protons and J_{HH} and J_{CH} coupling constants. The NOE interactions of exchangeable protons of NH and OH groups were observed in aqueous solution with the addition of deuterated acetone at a temperature of 260 K to decrease the rate of exchange of hydroxyl groups with water. Changes in mobility were examined by ^{13}C T_1 and T_2 measurements and performing a model-free analysis to obtain relevant relaxation parameters.

^{1}H NMR. Full assignments of the ^{1}H resonances of [c(ed)ba]$_n$ for n = 1, 2, 5, and 14 are given in Table 1. The chemical shifts are in good agreement with those reported previously for synthetic tetrasaccharide and sialopentasaccharide (Pozsgay et al., 1990, 1991). The ^{1}H assignment for native polysaccharide was incorrect for Glc-H3, which was reported to be 3.49 ppm. Identification of the glucose spin system by 1D TOCSY in the native polysaccharide revealed that at 290 K the protons H3, H4, and H5 form a strongly coupled system at 3.67 ppm (Figure 2). Only Glc-H3 in [c(ed)ba]$_1$, with the glucose in a terminal position, can provide the resonance in higher field, at 3.53 ppm. The direct comparison of the one and two repeat unit did not reveal any significant changes in the ^{1}H chemical shifts, although there were some minor differences in chemical shifts of GlcNAc and NeuAc residues depending on the proximity to the reducing Gal or internal Gal.

In order to establish the differences between the 3D structure of sialo, asialo, and modified compounds, their complete assignment was performed by 1D and and 2D TOCSY experiments (Tables 1 and 2). If there is conformational control of sialic acid over the residues in backbone, the removal of sialic acid may introduce some changes into the chemical shifts of backbone residues. 1D TOCSY analysis revealed that the only backbone residue affected by removal of sialic acid was Glc-H3, H5, and slightly GlcNAc-H4 (Figure 2). The comparison of the chemical shifts of

Table 1: ^{1}H Chemical Shifts[a] For Saccharides [c(ed)ba]$_n$ of GBS III and Desialylated GBSP III [c(d)ba]$_n$

			$n = 2$				
residue	H	$n = 1$[b]	I[c]	II[c]	$n = 5$[d]	$n = 14$[d]	[c(d)ba]$_n$
Gal (a)	1	4.569	4.571	4.447	4.431	4.435	4.43
Gal	2	3.54	3.54	3.61	3.59	3.59	3.58
Gal	3	3.72	3.72	3.75	3.73	3.71	3.73
Gal	4	4.17	4.17	4.18	4.17	4.17	4.17
Gal	5	3.70	3.70	3.70	3.70	3.71	3.69
Gal	6	3.74	3.74	3.74	3.74	3.74	3.75
Gal	6′	3.78	3.78	3.78	3.79	3.79	3.78
GlcNAc (b)	1	4.722	4.729	4.724	4.702	4.702	4.70
GlcNAc	2	3.82	3.82	3.83	3.82	3.81	3.81
GlcNAc	3	3.73	3.74	3.74	3.73	3.72	3.71
GlcNAc	4	3.91	3.90	3.90	3.91	3.93	3.91
GlcNAc	5	3.74	3.74	3.74	3.73	3.71	3.71
GlcNAc	6	3.97	3.97	3.97	3.98	3.96	3.98
GlcNAc	6′	4.30	4.31	4.31	4.29	4.29	4.27
Glc (c)	1	4.533	4.562	4.538	4.539	4.545	4.55
Glc	2	3.32	3.37	3.31	3.36	3.36	3.37
Glc	3	3.53	3.68	3.54	3.67	3.67	3.65
Glc	4	3.41	3.68	3.40	3.66	3.67	3.64
Glc	5	3.53	3.68	3.52	3.66	3.67	3.61
Glc	6	3.73	3.82	3.75	3.81	3.81	3.79
Glc	6′	3.94	4.00	3.94	3.99	4.00	3.98
Gal$_s$ (d)	1	4.627	4.632	4.632	4.611	4.621	4.55
Gal$_s$	2	3.58	3.58	3.58	3.57	3.57	3.54
Gal$_s$	3	4.11	4.11	4.10	4.10	4.10	3.67
Gal$_s$	4	3.98	3.98	3.98	3.97	3.97	3.92
Gal$_s$	5	3.71	3.71	3.71	3.70	3.69	3.69
Gal$_s$	6	3.74	3.74	3.74	3.74	3.74	3.75
Gal$_s$	6′	3.77	3.77	3.77	3.74	3.77	3.77
NeuAc (e)	3	2.758	2.762	2.762	2.752	2.758	
NeuAc	3′	1.833	1.833	1.829	1.814	1.821	
NeuAc	4	3.70	3.70	3.70	3.69	3.69	
NeuAc	5	3.87	3.87	3.87	3.86	3.86	
NeuAc	6	3.66	3.65	3.65	3.65	3.66	
NeuAc	7	3.62	3.61	3.61	3.61	3.61	
NeuAc	8	3.89	3.89	3.89	3.88	3.89	
NeuAc	9	3.88	3.88	3.88	3.88	3.88	
NeuAc	9′	3.66	3.66	3.66	3.65	3.66	

[a] In parts per million at 600 MHz, D_2O, pH 7.0, 290 K, and internal acetone at 2.225 ppm. [b] [c(ed)ba]$_1$ contains a mixture of α and β anomers of reducing galactose in a 1:4 ratio and minute quantities of an unknown α′ compound. The α anomers are not included because they were not relevant for further study. [c] I for the repeat unit at the reducing end and II for the terminal repeat unit. [d] The chemical shifts of signals from βGal reducing residue and Glc in terminal positions do not differ from the values observed for one and two repeat units.

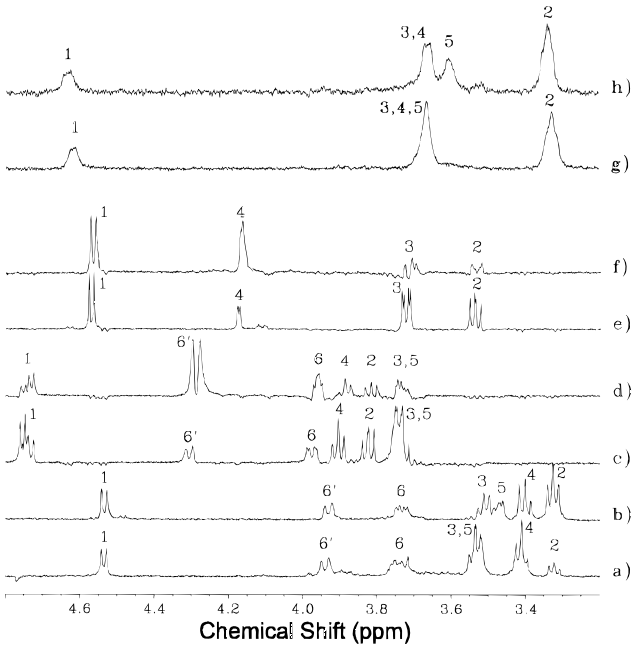

FIGURE 2: Comparison of 1D TOCSY ^{1}H 600 MHz spectra of ([c(ed)ba]$_1$ and [c(d)ba]$_1$) for Glc (a, b), GlcNAc (c, d), and Gal (e, f). The spectra for Glc in [c(ed)ba]$_{14}$ and [c(d)ba]$_n$ are shown in parts g and h. Only the Glc H3 and H5 and the GlcNAc H4 resonances showed significant displacement of chemical shift upon the removal of sialic acid.

Table 2: ^{1}H Chemical Shifts[a] Differences between the Native and Chemically Modified and Desialylated GBSP III

residue	H	native	NMe_4	reduced	oxidized	asialo
Gal	3	3.71	−0.02	−0.01	−0.02	−0.02
Gal	5	3.71	0	0	0.02	0.02
GlcNAc	4	3.93	−0.02	−0.01	−0.01	0.02
GlcNAc	6	3.96	−0.01	0	−0.01	−0.02
GlcNAc	6′	4.29	0	0	0.02	0.02
Glc	1	4.55	0	−0.03	−0.04	0
Glc	3	3.67	−0.01	−0.01	−0.03	0.02
Glc	4	3.67	−0.02	−0.01	−0.01	0.02
Glc	5	3.67	−0.02	0.05	0.04	0.06
Glc	6	3.81	0	0	0.01	0.02
Glc	6′	4.00	0.01	0.02	0.01	0.02
Gal_s	1	4.62	−0.02	−0.01	0.01	0.07
Gal_s	2	3.57	−0.01	0	0.02	0.03
Gal_s	3	4.10	0	−0.06	−0.01	0.43
Gal_s	4	3.97	−0.01	−0.08	−0.03	0.05
Gal_s	5	3.69	−0.01	−0.09	0.04	0
NeuAc	3	2.76	−0.01	0.56	0.06	
NeuAc	3′	1.82	−0.01	−0.12	0.05	
NeuAc	4	3.69	−0.01		0.05	
NeuAc	5	3.86	−0.01		0.14	

[a] In parts per million at 600 MHz, D_2O, pH 7.0, 290 K, and internal acetone at 2.225 ppm. Differences in all the compounds $<|0.02|$ are not shown.

Glc residues in sialo and asialopolysaccharides (Figure 2) again showed the influence on Glc-H5. Further examination of the modified polysaccharides with reduced and oxidized sialic acid confirmed that the modification on sialic acid induces long-range effects on chemical shifts of Glc-H3 and H4. The size of cations had no influence on the overall conformation, since upon replacement of the sodium cation by the tetramethylammonium cation no changes in chemical shift were observed.

The 1D TOCSY experiments enabled the accurate measurements of the majority of $^3J_{H,H}$ scalar coupling constants of [c(ed)ba]$_1$ and [c(d)ab]$_1$. Of particular interest were the coupling constants of methoxyl protons of the GlcNAc residue which is involved in the 1−6 linkage. For [c(ed)-ba]$_1$, $J_{5,6} = 3.9$ Hz and $J_{5,6'} = 1.8$ Hz, while for [c(d)ab]$_1$, $J_{5,6} = 4.2$ Hz and $J_{5,6'} = 1.2$ Hz, with an estimated error of ±0.1 Hz. The coupling constants for [c(ed)ba]$_1$ are in Table 3. From the coupling constants of the NeuAc residue, it can be concluded that the NeuAc residue adopts the $^2C_5$ chair conformation. For the NeuAc side chain, the coupling constants $^3J_{H6,H7} = 1.7$ Hz, $^3J_{H7,H8} = 9.7$ Hz, $^3J_{H8,H9} = 6.6$ Hz, and $J_{H9,H9'} = -12.1$ Hz are consistent with those reported previously (Acquotti et al., 1990).

Table 3: $J_{H,H}$ Coupling Constants (Hz) for Oligosaccharide [c(ed)ba]$_1$ of GBS III[a]

	$J_{1,2}$	$J_{2,3}$	$J_{3,4}$	$J_{4,5}$	$J_{5,6}$	$J_{5,6'}$
Gal	7.9	9.9	3.5	<1	nd[b]	nd
GlcNAc	8.5	8.5	10.5	8.6	3.9	1.8
Glc	8.4	8.6	9.5	9.6	5.6	2.4
Gal_s	7.8	9.7	3.2	<1	nd	nd

	$J_{3a,3e}$	$J_{3a,4}$	$J_{3e,4}$	$J_{4,5}$	$J_{5,6}$
NeuAc	12.4	12.2	4.7	10.3	10.5

	$J_{6,7}$	$J_{7,8}$	$J_{8,9}$	$J_{8,9'}$	$J_{9,9'}$
NeuAc	1.7	9.7	6.6	nd	12.1

[a] For [c(d)ba]$_1$ GlcNAc $J_{5,6} = 4.2$ Hz and $J_{5,6'} = 1.2$ Hz and for Glc $J_{5,6} = 5.8$ Hz and $J_{5,6'} = 1.8$ Hz. [b] Not determined.

An essential step in determining the conformational preference of the 1−6 linkage was the assignment of the prochiral protons at C6 of the branching GlcNAc residue. The assignment of H6$_R$ and H6$_S$ is based on NOE labeling, taking into account the spatial proximity of the H6$_R$ and H6$_S$ protons to H4 of the GlcNAc residue (Bock & Duus, 1994). The direct assignment of the pertinent protons from the 2D NOESY spectra was hampered by the severe spectral overlap of the H6$_R$ proton with other resonances. Also, the intensities of the NOE from H6$_S$ was affected by the fast transfer of magnetization between both methylene protons. To obtain the NOE from the proton H6$_R$, which lies in a crowded area, as well as to eliminate spin diffusion, the 1D selective relay−NOESY was performed for [c(ed)ba]$_1$. The magnetization was first transferred selectively by a COSY step from the H1 of GlcNAc, with a subsequent double relay step to GlcNAc-H4. During the second relay step a chemical shift selective filter was applied. The last step was an NOE transfer from H4, which revealed that the stronger NOE signal exists between the H6$_R$−H4 (data not shown). To avoid the undesirable magnetization transfer between methylene protons, a similar experiment was repeated, where during the mixing time of NOE transfer, an additional saturation pulse was applied to one of the C6 protons in order to stop one pathway of possible magnetization transfer. The shape of the multiplet H6$_R$ was broader, indicating that the saturation with the use of a selective pulse was not fully completed. Hence, the GlcNAc-H6′ signal at 4.30 ppm was assigned as H6$_S$ and the H6 one at 3.97 ppm as H6$_R$. On the basis of the vicinal coupling constants for $J_{5,6}$ and $J_{5,6'}$ for GlcNAc (Table 3), it was estimated that the CH_2OH group of the GlcNAc residue occupies about 75% of the $\omega = -60°$ rotamer and about 25% of the $\omega = 60°$ rotamer, with ω = (O6−C6−C5−O5) (Haasnoot et al., 1980).

Molecular Dynamics Simulations. In order to interpret the NMR parameters in terms of conformational models,

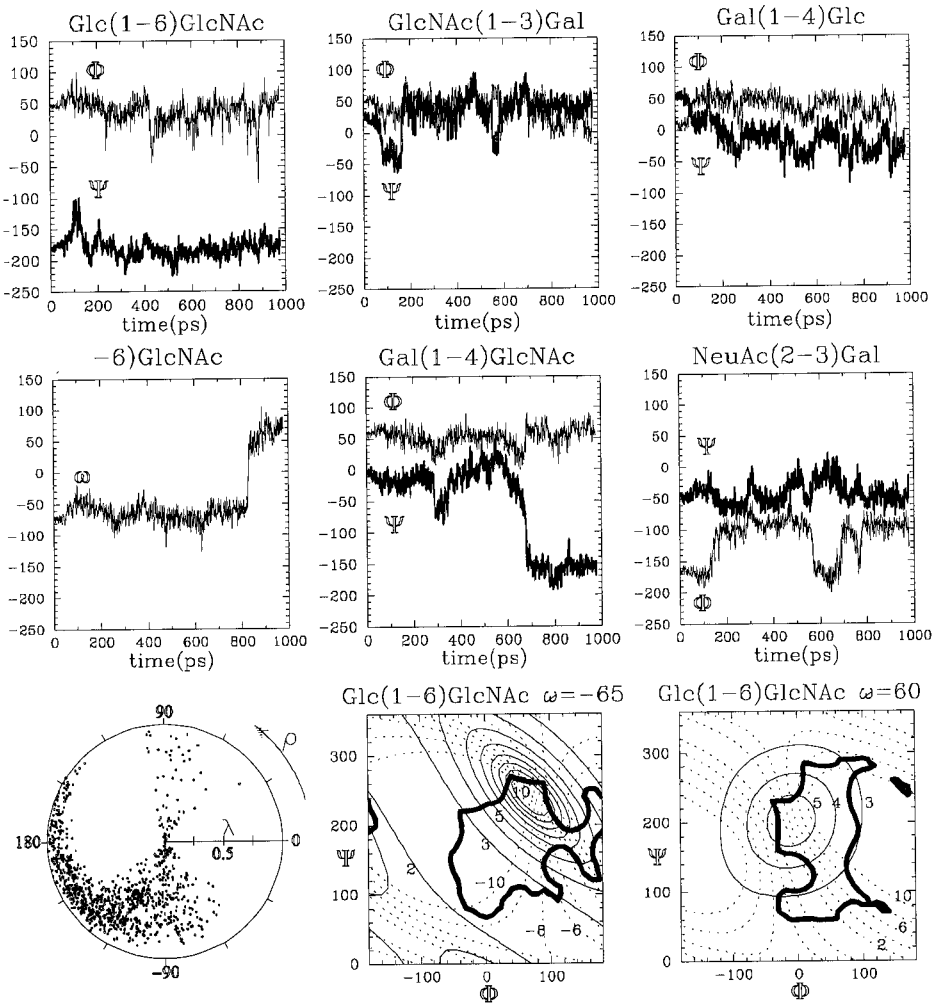

FIGURE 3: MD trajectories for the glycosidic torsion angles of $[ac(ed)ba]_1$. In the bottom row the polar (ρ, λ) representation of the distribution of (n, h) helical parameters calculated from the MD trajectory for $[ac(ed)ba]_1$ is shown, with n being the number of residues per turn, $\rho = 360°/n$, and λ is the percentage of maximum elongation (0 to 1). The helical parameters n (solid lines) and h (dotted lines) (Å) are also plotted as a function (Φ, Ψ) for the (1−6) linkage in $[bac]_2$ with $\omega = -65°$ and 60° along with the 6 kcal/mol contour level above the global PFOS energy minimum.

Table 4: Average Linkage Angles Obtained from the 0−1000 ps Molecular Dynamics Trajectories for Oligosaccharides of GBS III and Desialylated GBS III

residues		angle	$[ac(ed)ba]_1$	$[c(ed)ba]_1$	$[ac(d)ba]_1$	$[c(d)ba]_1$
Glc(1−6)GlcNAc	Φ	H1−C1−O1−C6	48 (14)	46 (14)	42 (21)	46 (16)
c−b	Ψ	C1−O1−C6−C5	−170 (18)	−170 (18)	−182 (17)	−174 (14)
b	ω	O6−C6−C5−O5	−65 (14)	−63 (12)	−59 (10)	−63 (11)
b	ω^a	O6−C6−C5−O5	60 (17)		51 (13)	
GlcNAc(1−3)Gal	Φ	H1−C1−O1−C3	40 (20)	39 (19)	48 (15)	43 (18)
b−a	Ψ	C1−O1−C3−H3	30 (28)	45 (19)	40 (17)	27 (33)
Gal(1−4)GlcNAc	Φ	H1−C1−O1−C4	52 (13)	44 (16)	50 (15)	26 (34)
d−b	Ψ	C1−O1−C4−H4	−12 (21)[b]	−21 (30)	−12 (26)[c]	−28 (25)
NeuAc(2−3)Gal	Φ	C1−C2−O2−C3	−43 (18)	−38 (20)		
e−d	Ψ	C2−O2−C3−H3	−116 (35)	−133 (35)		
Gal(1−4)Glc	Φ	H1−C1−O1−C4	37 (20)		45 (15)	
a−c	Ψ	C1−O1−C4−H4	−12 (30)		−7 (39)[d]	

[a] The $\omega = -60$ to $\omega = 60$ ratio was 80:20. [b] Averaged from 0 to 600 ps to exclude the $\Psi = 180$ conformer. [c] Averaged from 0 to 800 ps to exclude the $\Psi = 180$ conformer. [d] Averaged from 0 to 400 ps to exclude $\Psi = 180$ conformer.

molecular dynamics calculations were performed for single repeat units and for an additional Gal to obtain data for the Gal(1−4)Glc linkage. The MD 1000 ps trajectory for $[ac(ed)ba]_1$ is shown in Figure 3. The average linkage angles obtained from various MD runs of 1000 ps are shown in Table 4.

NOE Analysis. Proton 2D NOESY experiments were performed mostly at 290 K for the various compounds (Figure 4). Relevant NOE data are given in Table 5. Since all the linkages were β-D except for NeuAc, the intraresidue NOE for H1−H3 and H1−H5 interferred very often with the NOE across the glycosidic linkages. For the Gal(1−4)-Glc linkage, the H1a−H4c NOE could not be quantitated by itself since it overlapped with the H1a−H3a and H1a−H5a NOE. A similar situation occurred for GlcNAc(1−3)-Gal. To reduce line broadening and the effects of spin

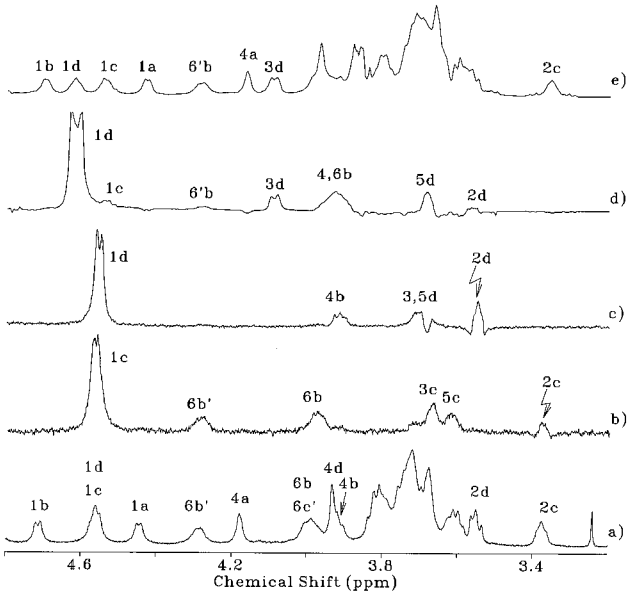

FIGURE 4: ^{1}H NMR spectrum of $[c(ed)ba]_{14}$ in e and desialylated GBS III PS $[c(d)ba]_n$ in a. The 1D selective TOCSY−NOESY of $[c(d)ba]_n$ with a selective transfer from Glc−H2c to Glc−H1c followed by a selective NOESY step is shown in b. The same experiment performed from Gal_s H2d (c). A NOE mixing time of 50 ms, a TOCSY mixing time of 20.5 ms, a half-Gaussian shaped 90° pulse of 70 ms, a 180° selective DANTE-Z pulse for the NOESY step of 10 ms, and 3200 and 2500 scans, respectively, were used in b and c. The NOE spectrum for H1d of $[c(ed)ba]_{14}$ from the 2D NOESY spectrum is shown in d.

diffusion, quantitative analysis of the NOEs was done on single repeat units when possible. For the Gal(1−4)Glc linkage measurement was done on $[c(ed)ba]_{14}$. For $[c(ed)ba]_1$ the measurements were recorded at 280 K with five mixing times in order to obtain the experimental NOE buildup curves. Of special interest was the area in the vicinity of the branching GlcNAc residue where the side chain NeuAc(2−3)Gal is attached to the backbone. Interresidue interactions from Gal_s −H1 to GlcNAc-H4, GlcNAc-H6 and GlcNAc-H6′ were observed (Figure 4). NOE interactions between Glc-H1, GlcNAc-H6, and GlcNAc-H6′ were detected as was an NOE from GlcNAc-H1 to Gal-H3 and Gal-H4. Of major significance was the NOE Glc-H1−Gal_s-H1 which suggested the interaction between the side chain and the Glc residue in backbone. This NOE was also observed for all the other $[c(ed)ba]_n$ oligosaccharides and the reduced and oxidized sialic derivatives (not shown).

The ensemble-averaged NOE calculated from the MD trajectories showed good agreement with the experimental NOE (Table 5). Since the errors on the experimental NOE were large due to overlap with other signals, it was difficult to assess whether any conformational changes were occurring due to structural variations. Also, since from the MD simulations the glycosidic linkages were fairly flexible with variations in Φ or Ψ with standard deviations from ±15° to ±30°, it would be difficult to determine if a unique set of conformers as opposed to ensemble averaging would satisfy the NOE constraints. This is because the NOE calculated for the virtual conformer generated from the average linkage angles from the MD simulation (Table 4) also showed good agreement with the experimental NOE. However, the standard deviation for the calculated NOE is very big for the interglycosidic NOE, which means that a wide range of rigid conformers would satisfy the NOE constraints.

Table 5: NOE Data for Oligosaccharides of GBS III

linkage	protons	$[c(ed)ba]_1$ exp[a]	$[c(ed)ba]_1$ calc[b]	$[c(ed)ba]_1$ calc[d]
Glc(1−6)GlcNAc	H1c−H2c	1.2	2.1 (0.2)	1.9
	H1c−(H3c + H5c)	9	13 (4)	13
	H1c−H6′b	2.2	3.4 (1)	3.2
	H1c−H6b	3.8	5.4 (1.5)	6
	H1c−H1d	1.4	1.7 (1.8)	0.5
GlcNAc(1−3)Gal	H1b−H2b	1.1	2.4 (0.3)	2.1
	H1b−(H3a + H3b + H5b)	16	19 (6)	18
	H1b-H4a	0.4	0.7 (0.3)	0.5
	H6′b−H6b	16	18 (1)	20
	H6′b−H4b	1.7	1.0 (0.2)	0.8
	H6′b−H5b	4.5	5.9 (1)	5
Gal(1−4)GlcNAc	H1d−H2d	1.5	2.3 (0.3)	2
	H1d−H3d	4.8	5.3 (1.9)	4
	H1d−H5d	7.6	6 (0.3)	7.2
	H1d−H4b	8.8	7 (2.6)	10
	H1d−H6′b	1	0.8 (0.6)	0.3
	H1d−(H6b + H4d)	2.7	2.7 (1.5)	1.4
NeuAc(2−3)Gal	$H3_{ax}e-H_{3eq}e$	16	20 (2)	22
	$H3_{ax}e-H4e$	2.9	3.1 (0.5)	3
	$H3_{ax}e-H5e$	3.3	5.1 (1.8)	5
	$H3_{ax}e-H3d$	2.5	4 (3)	2.5
	$H3_{eq}e-H4e$	5.5	5.8 (1.4)	5.3
	$H3_{eq}e-H5e$	0.8	2.3 (0.7)	2.1
	$H3_{eq}e-H3d$	0.8	1.9 (1.4)	1
		$[c(ed)ba]_{14}$ exp[a]	$[ac(ed)ba]_1$ calc[c]	$[ac(ed)ba]_1$ calc[d]
Gal(1−4)Glc	H1a−H2a	8	6 (1)	5
	H1a−(H4c + H3a + H5a)	93	58 (25)	66
	H1a−H6′c	6	14 (14)	7
	H1a−H6c	8	7 (7)	6

[a] Volumes from 2D NOESY with a mixing of 500 ms for $[c(ed)ba]_1$ and 100 ms for $[c(ed)ba]_{14}$, with a 50−100% relative error. The NOEs are relative to the H1d−H1d NOE for $[c(ed)ba]_1$ and the $H3_{ax}e-H3_{eq}e$ for $[c(ed)ba]_{14}$. [b] Ensemble averaged NOE using τ_c of 1 ns obtained from the fit of H1d−H1d NOE in the buildup curve. The standard deviation in parenthesis is calculated from the NOE at each point. [c] Ensemble averaged NOE using τ_c of 2 ns to fit the $H3_{ax}e-H3_{eq}e$ NOE. [d] NOE for the virtual conformer with the average linkage angles listed in Table 4.

This interresidue NOE was difficult to detect in asialo compounds because of the overlap between Gal_s-H1d and Glc-H1c even at different temperatures (Figure 4a). However, from a 1D selective TOCSY−NOESY experiment performed from the well-separated H2d and H2c resonances of Gal_s and Glc, it was possible to observe the NOE for the anomeric resonances of each residue. NOE signals from Glc-H1c (Figure 4b) were the similar to those of $[c(ed)ba]_{14}$. However, for $[c(d)ba]_n$ no NOE from Gal_s-H1d to H6b and H6′b of GlcNAc were detected (Figure 4c) as observed for $[c(ed)ba]_{14}$ (Figure 4d).

The orientation of sialic acid was probed by both 2D NOESY and 1D selective measurement (Siebert et al., 1992; Poppe et al., 1989). 2D NOESY crosspeaks were detected from NeuAc-$H3_{ax}$ to Gal-H3d and to Gal-H4d and between NeuAc-$H3_{eq}$ and Gal-H3d. To assess the conformation of the NeuAc(2−3)Gal linkage, an additional 1D selective TOCSY−NOESY experiment was performed (Figure 5) from the neuraminic acid glycerol side chain which was inaccessible from 2D NOESY spectra for reasons of signal overlap. The only resonance in the 1D spectrum which was reasonably isolated was NeuAc-H7. Thus, the TOCSY

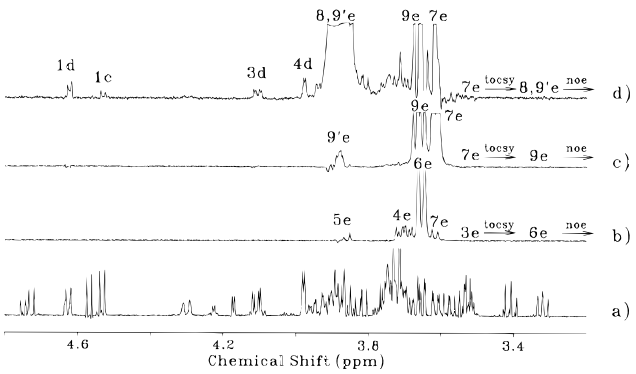

FIGURE 5: 1D TOCSY−NOESY for sialic acid of $[c(ed)ba]_1$ at 600 MHz. The ^1H spectrum with 16 scans is in a. In b, c, and d spectra were acquired using initial TOCSY transfer by a shaped 90° half-Gaussian (94 ms) followed by DANTE-Z pulse train of 16 ms, the TOCSY mixing time was 50 ms, including two trim pulses of 2.5 ms each, the NOESY mixing time was 300 ms, the relaxation delay 3 s, and 10 240 scans for each spectra.

transfer was performed from H7e to H8,9′e with a subsequent NOESY step produced by a DANTE Z pulse (Figure 5d). Hence, the NOE for the H8 and H9′ resonances (which overlapped) revealed the proximity of the H8 or H9′ protons to the H1d, H3d, and H4d of the neighboring Gal_s residue. These interactions could be explained in terms of multiple conformations around the 2−3 glycosidic bond. There was also a weak NOE between the sialic acid H8−H9′ and Glc-H1c. The experiment was repeated under slightly different conditions after lowering the temperature to 280 K and prolonging the mixing time in the NOESY step. This NOE signal was detected again, thus suggesting the proximity of the sialic acid side chain with Glc-H1 in the backbone. In the MD simulations, conformations were found which placed the NeuAc side chain in the vicinity of the Glc residue. From the MD simulations, the conformer with (Φ, Ψ) = (-169 ± 9, -40 ± 10) averaged from 0 to 400 ps in the MD run for $[ac(ed)ba]_1$ and was found to place the H8 and H9 protons close to the glucose ring, using the average angles for the other linkages. The other major conformer with (Φ, Ψ) = (-92 ± 13, -49 ± 16) flipped the sialic acid residue to put its NAc group close to the glucose ring (Figure 6). A similar 1D TOCSY−NOESY experiment (not shown) was performed from the Glc-H1 resonance to the Glc-H3,4,5 strongly coupled spin system. However, no NOEs with the sialic acid resonances were observed. Also, no NOEs between H6 of sialic acid (Figure 5b) and the proton resonances of the neigboring rings were detected.

The conformation of the NeuAcα(2−3)Gal linkage has been extensively studied previously in different oligosaccharides in both aqueous and nonaqueous solvents, and most of the results suggest that there is an inherent flexibility of this linkage, leading to exchange among several distinct conformations. In a recent report of the solution conformations of GM3 and GM4 gangliosides (Poppe et al., 1989; Siebert et al., 1992) it was concluded that the α(2−3) linkage can adopt two major conformations defined by the glycosidic dihedral angles very close to our values. For GM4 there was found one additional conformer in DMSO with (Φ, Ψ) = (61, −14) of which the presence was not confirmed in water. In a study (van Halbeek & Poppe, 1992) of the conformation and dynamics of a mucin glycoprotein derived diantennary octasaccharide, NeuAcα(2−3)Gal was again found to adopt only two conformations about this bond with

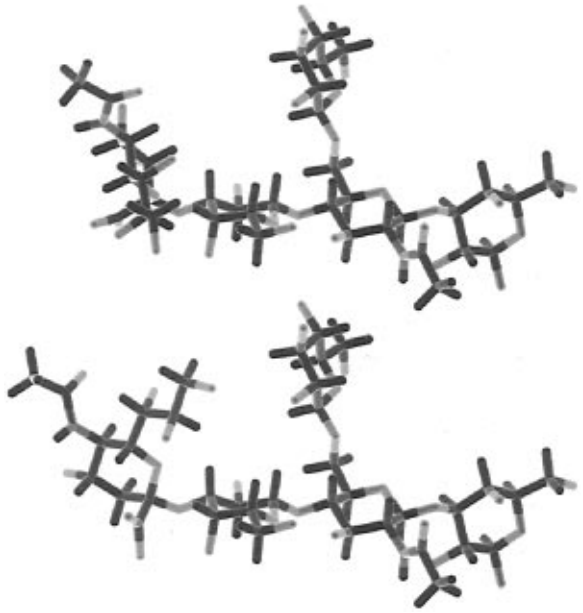

FIGURE 6: Average conformers for $[c(ed)ba]_1$ obtained using the average linkage angles from the molecular dynamic trajectories for $[c(ed)ba]_1$ with two orientations for sialic acid with (Φ, Ψ) = (−167, −40) (top) and (Φ, Ψ) = (−92, −49) (bottom) obtained from the 0−140 ps and 190−500 ps average over the MD run of Figure 3, respectively.

(Φ, Ψ) = (−170, −30) and (−85, 10). In a study of the GM2 fragment (Levery, 1991)the major conformer for this linkage was found to be (−167, −23), with the nonbonding interactions between GalNac and NeuAc shifting the energy balance toward this conformer. In contrast, the same linkage located at the branch point in GM1 was shown to be fairly rigid (Acquotti et al., 1990). Molecular dynamics simulations of the sialo $Lewis^X$ tetrasaccharide (Mukhopadhyay et al., 1994) showed several energy minima, two of which were close to our values of (Φ, Ψ) described previously. The NeuAcα(2−3) linkage in the sialo $Lewis^X$ tetrasaccharide is considered less flexible than in the disaccharide. Nevertheless, it is assumed that it undergoes rapid conformational fluctuations between at least three conformations. The conformation changes of sialo $Lewis^X$ upon binding to E-selectin were also reported (Cooke et al., 1994). Several other authors (Rodgers & Portoghese, 1994; Scarsdale et al., 1990) studied the conformational preferences of the various gangliosides. The conformation of the neuraminic acid glycerol side chain was studied by analyzing the relevant vicinal coupling constants and NOE, which were found to be in agreement with those reported previously.

^{13}C NMR. The NMR analysis of ^{13}C chemical shifts of oligosaccharide fragments (n = 2, 3, 5, poly) presented in Figure 7 and Table 6 revealed that some of the anomeric and aglycon carbons underwent a length dependent shift. This chemical shift difference was most significant for C4 of GlcNAc. The shape of its signal in the n = 5 repeat unit oligosaccharide is split into four individual lines created by every subunit, and in the polysaccharide this C4 signal was shifted by 0.5 ppm upfield, which was indicative of a slight change of the torsion angles of the inner subunits and the creation of unique conformational features.

A direct comparison of the one and two repeat units did not reveal any significant changes in the ^1H and ^{13}C chemical shifts, nor did it revealed unexpected NOE contacts. There were some minor differences in chemical shifts of GlcNAc

Table 6: ^{13}C chemical shifts[a] for saccharides [c(ed)ba]$_n$ of GBS III

			$n = 2$					
residue	C	$n = 1$	I[b]	II[b]	$n = 3$[c]	$n = 3$[d]	$n = 5$[e]	$n = 14$[e]
Gal (a)	1	97.27	97.28	103.74	103.80	97.38	103.80	103.92
Gal	2	71.60	71.61	70.80	70.87	71.70	70.85	70.82
Gal	3	83.19	83.21	82.82	82.94	83.29	83.02	83.32
Gal	4	69.07	69.09	69.03	69.13	69.15	69.12	69.09
Gal	5	75.51	75.50	75.67	75.75	75.59	75.74	75.78
Gal	6	61.79	61.70	61.79	61.86	61.79	61.86	61.87
GlcNAc (b)	1	103.56	103.7	103.7	103.80		103.89	103.97
GlcNAc	2	55.95	55.96	55.88	55.98		55.98	56.01
GlcNAc	3	72.83	72.77	72.81	72.87		72.82	72.85
GlcNAc	4	77.89	77.87	77.87	77.94		77.82	77.40
GlcNAc	5	74.01	74.09	74.04	74.14		74.11	73.90
GlcNAc	6	68.37	68.31	68.31	68.24		68.24	68.22
Glc (c)	1	103.52	103.37	103.54	103.47	103.63	103.44	103.44
Glc	2	73.74	73.40	73.75	73.48	73.80	73.47	73.42
Glc	3	76.39	75.01	76.40	75.09	76.50	75.09	75.12
Glc	4	70.35	78.96	70.39	79.04	70.48	79.07	79.23
Glc	5	76.55	75.42	76.56	75.51	76.65	75.51	75.53
Glc	6	61.46	60.76	61.48	60.86	61.55	60.85	60.86
Gal$_s$ (d)	1	102.90	102.90	102.9	102.99		102.96	102.87
Gal$_s$	2	70.12	70.12	70.12	70.22		70.20	70.23
Gal$_s$	3	76.48	76.42	76.42	76.56		76.51	76.59
Gal$_s$	4	68.41	68.31	68.31	68.40		68.41	68.43
Gal$_s$	5	75.76	75.77	75.77	75.86		75.85	75.85
Gal$_s$	6	61.83	61.84	61.84	61.94		61.94	61.76
NeuAc (e)	1	174.61	174.61	174.61	174.70		174.69	174.70
NeuAc	2	100.88	100.88	100.77	100.97	100.87	100.88	100.92
NeuAc	3	40.27	40.29	40.37	40.46	40.38	40.47	40.49
NeuAc	4	69.12	69.12	69.12	69.22		69.21	69.24
NeuAc	5	52.41	52.41	52.41	52.50		52.50	52.52
NeuAc	6	73.70	73.70	73.70	73.80		73.80	73.84
NeuAc	7	68.77	68.77	68.74	68.82		68.82	68.82
NeuAc	8	72.55	72.56	72.56	72.65		72.65	72.67
NeuAc	9	63.34	63.33	63.33	63.41		63.41	63.42

[a] In parts per million at 150 MHz, D_2O, pH 7.0, 290 K, and internal acetone CH_3 at 31.07 ppm. Only for compounds with βGal at the reducing end. For multiple conformers, the average chemical shift is given. [b] I for the repeat unit at the reducing end and II for the terminal repeat unit. [c] For internal residues. [d] For residues at the reducing or terminal end. [e] The signals of the reducing βGal and terminal Glc are not given due to their very low intensities.

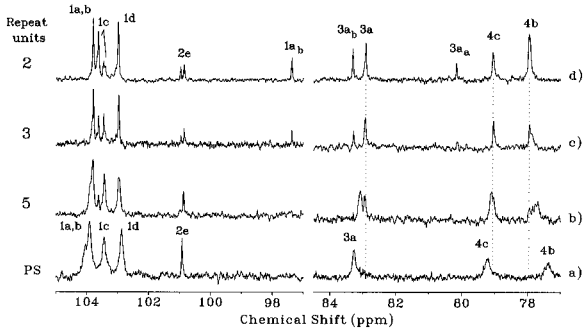

FIGURE 7: Gradual displacement of ^{13}C chemical shifts of the anomeric and linkage carbons for different number of repeat units, [c(ed)ba]$_n$, of GBS III. The linkage signals of C4 in GlcNAc moved gradually upfield from 77.9 ppm for $n = 2$ to 77.4 ppm for the polysaccharide (PS). The heterogeneity of the carbon signal GlcNAc−C4b is pronounced by its split character in the spectrum of the $n = 5$ repeat unit originating from the C4 signal of every individual GlcNAc residue. Downfield displacement was observed for Gal−C3a and Glc−C4c, and a minor change of chemical shift was observed for Gal$_s$−C1d. 3a$_a$ and 3a$_b$ refer to the C3 resonances of the αGal and βGal from the reducing end, respectively.

and NeuAc residues depending on the proximity to the reducing Gal or internal Gal. Sialic acid provided two sets of signals for C2, C3, and C7 in two repeat units, but this effect was not translated to the neighboring Gal$_s$.

Comparison of the ^{13}C chemical shifts of the native and desialylated PS and OS of GBS III is given in Table 7. Previous authors correlated the serological specificity of the native type III antigen with its structural and conformational features and noted the displacement of the aglycon carbon GlcNAc-C4 in sialylated and desialylated PS (Pozsgay et al., 1991; Jennings et al., 1984). Though conformation dependent shifts are difficult to interpret quantitatively, it is well-known that the differences in glycosylation shifts and the size of heteronuclear coupling constant $^3J_{CH}$ have strong correlation with molecular conformation. This dependence, represented by a calibration curve, correlates ^{13}C chemical shifts of the anomeric and aglycon carbon atoms with the glycosidic dihedral angle Ψ (Bock et al., 1986). According to this curve, a change of 10° in the time-averaged Ψ angle causes a 1−2 ppm change in the ^{13}C aglycon chemical shift. In a recent study on *S. pneumoniae* serogroup 9 capsular PS, minor differences in glycosylation shifts were observed at the sites of structural variations (Rutherford et al., 1994).

A systematic examination of all ^{13}C conformation dependent shifts in this work revealed differences due to the presence of sialic acid. The glycosylation shifts of GlcNAc-C4 differ by −0.5 ppm, Gal-C3 by 0.5 ppm, and Glc-C4 by 0.3 ppm, and differences of about 0.2 ppm were observed for anomeric carbons GlcNAc-C1 and Gal$_s$-C1.

The variable temperature measurement of sialo and asialo PS indicated significant changes in the ^{1}H and ^{13}C chemical shifts of the GlcNAc residue. The ^{13}C chemical shifts of C1, C4, and C6 of GlcNAc varied by up to 0.5 ppm between

Table 7: ^{13}C Chemical Shifts[a] of Desialylated Polysaccharide (PS) and $[c(d)ba]_n$ for $n = 1$, 5 and Difference in Chemical Shifts Δ_n between $[c(ed)ba]_n$ and $[c(d)ba]_n$

residue		$n = 1$	Δ_1	$n = 5$	Δ_5	PS	Δ_{PS}
Gal (a)	1	97.37	0.10	103.77	0.03	103.71	0.21
Gal	2	71.69	0.09	70.81	0.04	70.80	0.02
Gal	3	83.30	0.11	82.96	0.06	83.06	0.26
Gal	4	69.18	0.11	69.07	0.05	69.07	0.02
Gal	5	75.60	0.09	75.74	0.0	75.76	0.02
Gal	6	61.81	0.02	61.84	0.02	61.84	0.03
GlcNAc (b)	1	103.64	0.08	103.81	0.08	103.81	0.16
GlcNAc	2	56.21	0.26	55.98	0.0	56.01	0.0
GlcNAc	3	72.95	0.12	72.85	0.03	72.84	0.01
GlcNAc	4	78.33	0.44	78.20	0.38	78.21	0.81
GlcNAc	5	74.07	0.06	74.07	0.04	74.07	0.17
GlcNAc	6	68.28	0.09	68.20	0.04	68.25	0.03
Glc (c)	1	103.58	0.06	103.51	0.07	103.44	0.0
Glc	2	73.81	0.07	73.44	0.03	73.47	0.04
Glc	3	76.44[b]	0.05	75.05	0.04	75.08	0.04
Glc	4	70.50	0.15	79.16	0.09	79.14	0.09
Glc	5	76.69[c]	0.14	75.56	0.05	75.56	0.03
Glc	6	61.54	0.08	60.84	0.01	60.85	0.01
Gal_s (d)	1	103.54	0.64	103.40	0.44	103.52	0.65
Gal_s	2	71.75	1.63	71.73	1.53	71.74	1.51
Gal_s	3	73.26	3.22	73.26	3.25	73.28	3.31
Gal_s	4	69.42	1.01	69.41	1.0	69.42	0.99
Gal_s	5	76.09	0.33	76.08	0.23	76.10	0.25
Gal_s	6	61.95	0.11	61.94	0.0	61.95	0.19

[a] In parts per million at 150 MHz, D_2O, pH 7.0, 290 K, and internal acetone CH_3 at 31.07 ppm. Only for compounds with βGal at the reducing end. [b] Assignments may be interchanged.

290 and 315 K, while a smaller variation was observed for Glc-C4. Chemical shifts are sensitive to changes in time-averaged conformations of polysaccharides which are usually temperature dependent. The branched GlcNAc residue could be involved in conformational changes that occur with a change in temperature.

$^3J_{CH}$ Coupling Constants. The possible changes in torsion angles were further examined by measurement of $^3J_{C,H}$ coupling constants across glycosidic linkages and by MD simulation of these experimental parameters. The $^3J_{CH}$ coupling constants of $[c(ed)ba]_n$ with $n = 1$ and 3 and $[c(d)ba]_1$ are listed in Table 8. The magnitude of interglycosidic $^3J_{CH}$ couplings can be related to the torsion angles (Φ, Ψ) about the glycosidic linkages by a Karplus type equation. The biggest value of $^3J_{CH}$ was observed between Gal-C1d and GlcNAc-H4b (5.3 Hz) for $[c(ed)ba]_1$, which, together with strong NOEs between the protons Gal-H1d and GlcNAc-H4b, pointed to a high distribution of conformers with the torsion angle Ψ close to 0°. The same conformation was observed by MD simulation for $[c(ed)ba]_1$ where $\langle\Psi\rangle = -21° \pm 30°$ (Table 4) and a calculated value of $J_\Psi = 5.0 \pm 1.2$ Hz. The corresponding experimental coupling constant for $[c(d)ba]_1$ was found to be only 4.6 Hz, which indicated a possible change of the torsion angle Ψ for that linkage. However, the calculated value of $J_\Psi = 4.9$ Hz for $[c(d)ba]_1$ did not reflect a corresponding change of the Ψ distribution in the MD trajectory (see below). There was no other significant difference observed for the experimental J_{CH} between the sialo and asialo compounds. An additional coupling constant, present only in the $n = 3$ repeat unit, was observed between Glc-C4 and Gal-H1, with a value of $J_\Phi = 2.2$ Hz, which corresponded to Φ about 60° for the Gal-(1−4)Glc linkage. The other coupling constants of three repeat units were difficult to extract because of the broad character of the multiplets.

Significant differences were observed between the experimental and MD-simulated values of both sialo and asialo compounds. J_Φ for Gal(1−4)GlcNAc was near 4.0 Hz, whereas the average calculated value was near 2.5 Hz, with a standard deviation of 1 Hz. Since, from the MD simulation, $\langle\Phi\rangle = 44 \pm 16°$ (Table 4), this indicated that conformers near $\Phi = 20 \pm 10°$ (Figure 3) should be more highly populated in order to increase the average value of J_Φ. Similarly, J_Ψ for the Glc(1−6)GlcNAc linkage was near 4 Hz with calculated values near 2 Hz. Again this indicated that conformers with Ψ near −100° or near −210° should be more highly populated (Figure 3), since these conformers have J_Ψ values from 4 to 5.5 Hz. In some MD simulations a significant contribution from conformers with Ψ close to 180° was also observed (Figure 3). The unexpected presence of this conformer may suggest that the time scale for the simulations was too short to generate accurate conformational distributions for all linkages. Alternatively, the need for carbohydrate specific torsion terms in the GLYCAM parameters for Ψ may be needed.

^{13}C T_1 and T_2. The ^{13}C-relaxation T_1 and T_2 measurements were performed at 290 K for the one repeat unit sialo and asialo OS as well as on their PS counterparts (Table 9). The experiment was optimized for $^1J_{CH} = 150$ Hz, and the refocusing delay was set for CH coupling, so the CH_2 carbons were not detected. The ^{13}C-relaxation data for $[c(ed)ba]_1$ do not point to major differences between T_1 values for side chain residues (Gal_s, NeuAc) and branching GlcNAc residue carbons. The increased molecular mobility was observed for reducing Gal and Glc which is conferred by their terminal position and thus increased flexibility.

The relaxation data for NeuAc indicated that the mobility of the glycerol side chain and the ring carbons was similar. The restricted mobility was observed especially for C7, which is assumed to be hydrogen bonded to the N-acetyl group of

Table 8: $^3J_{CH}$ Coupling Constants (Hz) across the Glycosidic Linkages for Saccharides of GBS III and Desialylated GBS III

			$[c(ed)ba]_1$		$[c(d)ba]_1$	
linkage	C, H	J	exp[a]	calc[b]	exp[a]	calc[b]
Glc(1−6)GlcNAc	C6b, H1c	J_Φ	4.3	3.3 (1.3)	4.3	3.0 (1.2)
	C1c, H6′b	$J_{\Psi'}$	4.2	1.9 (1.0)		
	C1c, H6b	J_Ψ	3.8	1.9 (1.0)		
GlcNAc(1−3)Gal	C3a, H1b	J_Φ	4.6	3.2 (1.5)	4.9	2.7 (1.2)
	C1b, H3a	J_Ψ	3.7	3.5 (1.3)		
Gal(1−4)GlcNAc	C4b, H1d	J_Φ	4.0	2.3 (1.2)	4.3	2.5 (1.1)
	C1d, H4b	J_Ψ	5.3	5.0 (1.2)	4.6	4.9 (1.5)
			$[c(ed)ba]_3$	$[c(ed)ba]_3$		
Gal(1−4)Glc	C4c, H1a	J_Φ	2.2	3.4 (1.3)		

[a] Estimated error of ±0.1 Hz. [b] $\langle J_{CH}\rangle$ average calculated from the appropriate MD trajectories. The standard deviation is in parenthesis.

Table 9: T_1 and T_2 ^{13}C Values (ms) for Saccharides of GBS III and Desialylated GBS III

		T_1				T_2	
residue	C	[c(ed)ba]$_1$	[c(d)ba]$_1$	[c(ed)ba]$_{14}$	[c(d)ba]$_n$	[c(ed)ba]$_1$	[c(d)ba]$_1$
Gal	1	439	360	681	539	292	270
Gal	2	425	291[a]	570	533	278	280[e]
Gal	3	352	310	404	934	nd[h]	211
Gal	4	389	305	649	704	259	316
Gal	5	383	440	526[d]	624	nd	280
GlcNAc	1	325	208	741	883	263	194
GlcNAc	2	327	265	483	551	235	243
GlcNAc	3	383	268	478	678	nd	334
GlcNAc	4	261	244	574	805	166	227
GlcNAc	5	248	232	564	328	234	179
Glc	1	348	283[b]	509	545	267	226[f]
Glc	2	342	301	567	693	285	331
Glc	3	337[c]	284	544	961	276[g]	363
Glc	4	365	267	495	412	258	310
Glc	5	337[c]	280	526	501	276[g]	315
Gal$_s$	1	311	283[b]	426	545	207	226[f]
Gal$_s$	2	312	291[a]	475	630	228	280[e]
Gal$_s$	3	283	365	421	911	233	275
Gal$_s$	4	299	265	570	691	nd	296
Gal$_s$	5	326	355	526[d]	574	nd	262
NeuAc	4	295		437		nd	
NeuAc	5	314		408		220	
NeuAc	6	293		391		212	
NeuAc	7	266		425		200	
NeuAc	8	323		498		213	

[a–g] The relaxation of overlapping signals is the same and is indicated by identical superscripts. [h] Not determined due to noise in the F1 domain.

sialic acid. The slightly increased mobility of C8 might suggest the weaker character of the second hydrogen bond. These relaxation data agree with the T_1 measurement observed previously on a sialopentasaccharide (Pozsgay et al., 1990). The restricted mobility of these carbons was reported previously (Breg et al., 1989), and the relaxation times of the C7 and C8 of their compound were almost identical.

T_1 and T_2 values of the sialo and asialo PS also revealed some differences in their overall tumbling. The average T_1 values of asialo PS suggest identical overall mobility for all monosaccharide residues, though it is necessary to point out that the higher molecular weight of asialo PS and the broader character of the signals might introduce bigger deviations of the observed intensities of the signals from the fitted curve. For [c(ed)ba]$_{14}$ a different mobility for the backbone and the side chain was observed. It is worthwhile noting the slightly decreased mobility of the Glc residue, which might be due to hydrogen bonding.

The relaxation data were analyzed in terms of the model-free formalism (Lipari & Szabo, 1982b) (Table 10). In all cases the overall motion was found to be isotropic. Both T_1 and T_2 for all positions were well-fitted by the parameters given in Table 10 indicating that it is unlikely that there is conformation conversion on the millisecond time scale. For [c(ed)ba]$_1$ and [c(d)ba]$_1$, overall correlation times were found to be 0.76 and 0.54 ns, respectively. The generalized order parameter S is a measure of the amplitude of local motions with a value of 1, indicating little or no motion, while a value of 0 indicates essentially unrestricted motion. Inspection of Table 10 suggests that for [c(d)ba]$_1$ the GlcNAc residue is undergoing motion of significantly smaller amplitude than the other constituent residues. This most likely reflects influence of the branching residues on its local motions. The terminal Gal, Gal$_s$, and Glc residues have similar order parameters. Sialylation of the Gal$_s$ residue attenuates the motional fluctuation of the pyranose ring when compared to Gal$_s$ of the asialo counterpart. Surprisingly, the NeuAc residue shows order parameters comparable to those of the internal residues, suggesting that motion about NeuAc(2−

Table 10: Relaxation Parameters[a] for Saccharides of GBS III and Desialylated GBS III

	[c(ed)ba]$_1$		[c(d)ba]$_1$		[c(ed)ba]$_n$		[c(d)ba]$_n$	
	S^2	τ_i (ps)	S^2	τ_i (ps)	S^2	τ_i (ps)	S^2	τ_i (ps)
Gal								
1	0.53	6.2	0.71	4.7	0.35	42	0.43	43
2	0.54	6.2	0.76	6.4	0.49	44	0.53	33
3	0.66	6.2	0.89	4.9	0.93	41	0.18	31
4	0.60	6.1	0.68	14	0.40	40	0.29	35
5	0.61	6.1	0.65	4.3	0.56	47	0.37	36
GlcNAc								
1	0.71	6.2	0.99	5.7	0.27	43	0.20	32
2	0.71	6.2	0.86	5.6	0.66	45	0.47	34
3	0.61	5.9	0.60	71	0.66	46	0.27	41
4	0.91	6.0	0.94	5.7	0.52	42	0.23	34
5	0.95	6.0	0.99	5.4	0.49	45	0.97	40
Glc								
1	0.67	6.2	0.88	5.8	0.54	51	0.45	39
2	0.68	26	0.64	30	0.51	41	0.31	34
3	0.69	6.2	0.52	77	0.57	41	0.13	35
4	0.64	6.0	0.72	28	0.58	49	0.74	31
5	0.69	6.2	0.69	25	0.63	38	0.54	37
Gal$_s$								
1	0.76	6.0	0.88	5.4	0.82	46	0.49	33
2	0.75	6.2	0.71	34	0.68	45	0.38	33
3	0.82	6.2	0.70	5.0	0.89	41	0.17	34
4	0.78	6.3	0.70	47	0.54	39	0.32	33
5	0.72	6.2	0.73	4.8	0.62	40	0.44	35
NeuAc								
4	0.79	6.2			0.77	46		
5	0.74	6.1			0.85	50		
6	0.80	6.2			0.96	41		
7	0.88	6.2			0.88	38		
8	0.72	6.0			0.69	37		

[a] Correlation times $\tau_1 = \tau_2$ reflected overall isotropic motion, 0.76 ± 0.04 ns for [c(ed)ba]$_1$, 0.54 ± 0.04 ns for [c(d)ba]$_1$, 2.2 ± 0.03 ns for [c(ed)ba]$_n$, and 2.8 ± 0.04 ns for [c(d)ba]$_n$.

3)Gal_s is significantly constrained compared to that experience by the terminal Glc and Gal residues. If we assume that motion about the glycosidic linkages may be crudely represented as a libration of the pyranose rings in a cone of semiangle Θ_0, then the order parameter is given by (Lipari & Szabo, 1980)

$$S_{\text{cone}} = \frac{1}{2}(\cos\theta_0(1 + \cos\theta_0)$$

so that the semicone angle is then given by

$$\theta_0 = \cos^{-1}\left(\frac{1}{2}(1 + 8S_{\text{cone}})^{1/2} - 1\right)$$

Using this model and the order parameters of the sialo and asialo repeating unit, Θ_0 values of 23° and ~4° are calculated for the GlcNAc residues, respectively. Inspection of the MD trajectory for the Φ and Ψ angles of the GlcNAc-(1−3)Gal linkage and the Ψ of the Glc(1−6)GlcNAc and Gal_s(1−4)GlcNAc linkages (Figure 3) suggests that the torsion angles fluctuate on average by approximately ±20°, suggesting that the calculated values Θ_0 can be used as indicators of the degree of flexibility of the glycosidic linkages. Interestingly, the NeuAc residue has an order parameter which is comparable to the internal GlcNAc and Gal_s residues. The MD trajectory suggests that large fluctuations in the Φ and Ψ angles may be occurring. This discrepancy could reflect that the assumption above is not justified or that NeuAc is not as well-handled by the force field used in the MD calculations as are the neutral carbohydrate residues. It is intriguing that the GlcNAc residue becomes more mobile on going from the asialo to the sialo repeat unit.

On fitting the relaxation data for the polysaccharides, overall isotropic motion was found for $[c(ed)ba]_{14}$ and $[c(d)ba]_n$ with correlation times of 2.2 and 2.8 ns, respectively. In the case of $[c(d)ba]_{14}$ the order parameters are much less for all residues compared with those of $[c(d)ba]_1$. In addition the rates of internal motion τ_i are nearly an order of magnitude slower. If the internal motion is assumed to be libration in a cone of semiangle Θ_0, the GlcNAc residues in the asialo PS would be fluctuating with an amplitude of ±49° ($\langle S^2\rangle = 0.29$) while in $[c(d)ba]_1$ the amplitude is ±4° ($\langle S^2\rangle = 0.88$). In contrast, the corresponding residues in the sialylated $[c(ed)ba]_{14}$ and in $[c(ed)ba]_1$ exhibit a less dramatic difference in order parameters. In particular the GlcNAc residue has an average S^2 value of 0.78 for $[c(ed)ba]_1$ and 0.52 for $[c(ed)ba]_{14}$. This corresponds to an increase in librational amplitude of the pyranose ring from $\Theta_0 \pm 23°$ in $[c(ed)ba]_1$ to $\Theta_0 \pm 37°$ in $[c(ed)ba]_{14}$. As with the desialylated PS the internal motion occurs on a time scale which is about an order of magnitude longer than those of the single repeat unit. From the relaxation data it appears that the presence of the negative charge on the sialyl group constrains flexibility along the polysaccharide chain as compared with that in the asialo polysaccharide.

Hydroxyl Protons. The exchangeable protons of the hydroxyl groups and acetamido groups in aqueous solutions can give additional information about dipole−dipole contacts and hydrogen bonding which is not accessible from NMR in deuterated water. Several groups recently reported success in observing hydroxyl protons by lowering the temperature to slow exchange and by using pulse sequences that suppress the water signals (Adams & Lerner, 1992; Leeflang & Vliegenthart, 1990; Poppe & van Halbeek, 1991). The measurement of hydroxyl groups in aqueous and nonaqueous solutions was attempted, but the latter approach was hindered by the low solubility of the sialo compounds in dimethyl sulfoxide.

Table 11: Chemical Shifts[a] and Temperature Coefficient[b] of the Resolved Hydroxyl Resonances of the Synthetic Pentasaccharide $[c(ed)ba]_1$ of GBS III

	chemical shift (ppm)	temp coeff. (ppm/K)
Gal−OH2	6.650	0.012
Gal−OH4	5.979	0.011
GlcNAc−OH3	6.150	0.011
Glc−OH2	6.615	0.012
Glc−OH3	6.067	0.012
Gal_s−OH2	5.797	0.010
Gal_s−OH4	6.021	0.012
NeuAc−OH4	6.401	0.010
NeuAc−OH7	5.793	0.009
NeuAc−OH8	6.202	0.008
NeuAc−NH	8.323 (8.6)[c]	0.006
GlcNAc−NH	8.492 (8.6)[c]	0.007

[a] In ppm at 600 MHz, for solution in 65% H_2O and 35% acetone-d_6 at 265 K, and internal acetone at 2.225 ppm. [b] The temperature dependence was observed over a 15 K range from 280 to 265 K. [c] $J_{NH,H}$ coupling constants in Hz.

The spectra of one and three repeat units sialopentasaccharide and asialotetrasaccharide showed NH signals at 8.2−8.6 ppm. Hydroxyl signals of the sialo compound were observed between 7.0 and 5.6 ppm at 260 K. Some of these signals were well-resolved and sharp, but it was not feasible to extract coupling constants. Thus, the use of 2D techniques to trace the *J* connectivity was limited to transfer across one coupling constant, from hydroxyl proton to the neighboring ring proton. The hydroxyl protons of $[c(d)ba]_1$ were undetectable even at low temperature, which might be due to the faster exchange of these protons due to different solvation effect of the sample without sialic acid. The NH coupling constants were identical (8.6 Hz) and were typical of free NH protons with very similar temperature coefficients (Table 11). The temperature coefficients of the hydroxyl protons were slightly higher and were almost uniform near 0.010 ppm/K.

Traces of the 1D NOE difference spectra of the OH resonances are shown in Figure 8b−h, along with the basic jump and return spectrum in Figure 8a for $[ac(ed)b]_1$. The assignment of the OH resonances was based on the 1D steady-state NOE combined with jump and return 2D TOCSY. The tentative assignment of the GlcNAc-OH3 group is depicted by an asterisk in Figure 8a, since no crosspeak was observed in the 2D TOCSY spectrum. However, dipolar connectivities were observed to GlcNAc-H2, H3, and H4 resonances (Figure 8f). In Figure 8b, the Gals-OH2 and NeuAc-OH7 overlapped and NOE contacts to both the Gal_s and NeuAc residues were identified. Figure 8, panels c, d, and e show NOE contacts of hydroxyl protons to a neighboring ring proton. Hydroxyl groups Glc-OH3 (Figure 8e) and Glc-OH2 (Figure 8h) show the same connectivity to Glc-H3, but the hydroxyl resonance at 6.65 ppm showed a TOCSY peak to Glc-H2 and was thus assigned to Glc-OH2. The signal 2a in Figure 8h arises due to partial irradiation of Gal-OH2.

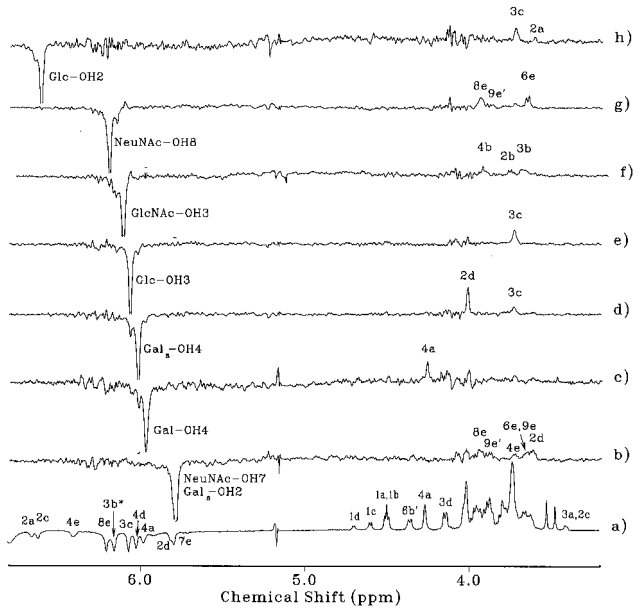

FIGURE 8: ^{1}H NMR spectra of [ac(ed)b]$_1$ recorded in H_2O:acetone-d_6 (65:35, v:v) at 600 MHz and 260 K, using the 1−1 spin−echo sequence (a) and 1D steady-state NOE difference spectra (b−h) after selective irradiation of hydroxyl protons resonances for 0.7 s and using the 1−1 spin−echo sequence for the read pulse. The interpulse delay in the spin−echo sequence was 400 μs and the number of scans in each spectrum was 2048.

The NOE spectra for Gal-OH2 and NeuAc-OH4 are not shown due to the poorer quality of the spectra due to faster relaxation of these residues resulting in broader lines, especially for NeuAc-OH4. The assignment for NeuAc-OH4 was verified from 2D TOCSY, where crosspeaks between NeuAc-OH4 and the ring H4 and H5 resonances were observed. It should be mentioned that the similar signal in a biantennary oligosaccharide (van Halbeek & Poppe, 1992) was assumed to belong to NeuAc-OH9, but the authors concluded that the assignment was ambiguous.

Five OH resonances showed significantly sharp signals, among them OH7 and OH8 of sialic acid. The study of hydroxyl groups of biantennary octasaccharide (van Halbeek & Poppe, 1992) performed under similar conditions revealed only one sharp intense signal, which had been assigned to NeuAc-OH8. It showed the smallest temperature coefficient, suggesting slower exchange with the bulk water and a possible hydrogen bond with the carboxylate group. In our case, on the contrary, for the sialiopentasaccharide, several sharp and well-resolved hydroxyl signals with almost identical temperature coefficients were observed with slightly lower values for the NH resonances and the OH7 and OH8 signals of sialic acid.

Helical Parameters. The helical parameters for the repeat unit of GBS III were calculated from the molecular dynamics trajectories of [ac(ed)ba]$_1$ which comprises the single repeat and the additional Gal(1−4)Glc linkage that joins two units together. The single unit was then extended, thus forming a helix with distinct helical parameters. These local helices help describe the spatial organization of the polysaccharide and allow an interpretation of whether extended conformations are feasible. The helical parameters were represented in a polar (ρ, λ) map adequate to compare at a glance the secondary structures displayed by native and asialo GBS III polysaccharides. As can be observed in Figure 3, GBSP III can form a wide range of helices, some of which are quite extended with $n > 4$ ($|\rho| < 90$) and $\lambda > 0.5$. A similar distribution of helical parameters was found for the desialylated GBS III using data from the [ac(d)ba]$_1$ MD trajectory. The helix parameters obtained from the average linkage angles and $\omega = -65°$ given in Table 4 for [ac(ed)ba]$_1$ was $n = 3.3$ and $\lambda = -0.8$ and $n = 3.3$ and $\lambda = -0.7$ for [ac(d)ba]$_1$. The helical parameters are also shown as a function of (Φ, Ψ) and $\omega = -65°$ and $-60°$ for the 1−6 linkage with the linkage angles fixed to minimum PFOS energy conformers (Φ, Ψ) = (10, 40) and (40, 20) for the GlcNAc(1−3) linkage and Gal(1−4) linkage, respectively. Changing the linkage angles over the range of allowed conformers for the GlcNAc(1−3)Gal(1−4)Glc linkages would not alter significantly the overall (n, h) map. For $\omega = -65°$ for a wide range of (Φ, Ψ), small changes in angles ($\pm 20°$) can lead to large changes in helical parameters. For $\omega = 60°$, extended conformations with $n = 5$ are also possible but of opposite chirality. Such extended helices are shown in Figure 9 for $n = 5$, $h = -11$ Å, and $\lambda = -0.75$ and for $n = 5$, $h = 10.5$ Å, and $\lambda = 0.8$.

DISCUSSION

The role of sialic acid in defining the proposed conformational epitope of group B *Streptococcus* type III capsular polysaccharide can be rationalized in terms of conformational features determined from this study. Sialic acid was found to exert control over the conformational features of the backbone. For the one repeat unit [c(de)ba]$_1$ of GBS III, most structural changes upon the removal of sialic acid were determined to occur at the branching point, since changes in chemical shifts, NOE, and $^3J_{CH}$ occurred in signals of resonances in the vicinity of the branching point. Changes in mobility in the backbone and different OH exchange rates were observed upon the removal of sialic acid. Similar structural changes for the polysaccharide upon removal of sialic acid were observed.

While the carboxylate group of the sialic acid is essential to the formation of the epitope, other structural features are not (Jennings et al., 1981). Reduction of sialic acid induced long-range chemical shift changes on the Glc residue, indicating possible changes in the anisotropic environment, changes in the backbone conformation, or a different orientation of sialic acid with respect to the backbone. Conformational changes are preferred because oxidized sialic acid which retained the carboxylate groups had no effect on the serology (Jennings et al., 1981) and also induced chemical shift changes on Glc. These changes can be explained by the proximity of the C8−C9 groups to the Glc residue for some allowed conformations, one of which in shown in Figure 6.

Molecular dynamics simulations were performed to develop models to interpret the NMR and serological results. Overall the simulation of observable NMR parameters was well-reproduced by the MD simulations. The ensemble average NOE calculations were in good agreement with the experimental NOE. Although multiple unique rigid conformers could be found which also reproduce the observed NOEs, no justification for a unique conformer could made, since the error of the measurement and the wide fluctuations in the calculated NOE at each point of the whole trajectory were similar. Although the simulation of the $^3J_{CH}$ coupling constants showed more disparity, slight changes in the

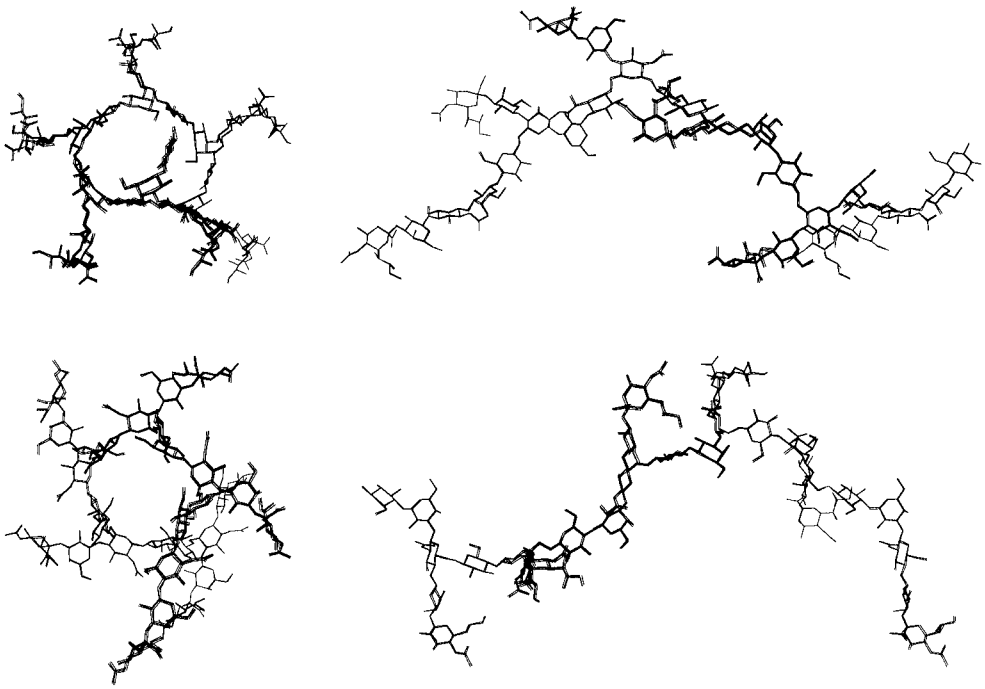

FIGURE 9: Side and top view of two $n = 5$ helices of $[(ed)bac]_6$ with $\omega = -65$ (bottom) and $\omega = 60$ (top) for the (1−6) linkage, which have extended conformations.

population of allowed conformers would reproduce the observed $^3J_{CH}$ for the glycosidic linkages. The (Φ, Ψ) distribution for sialic acid generated a model for the interaction sialic acid with the Glc unit (Figure 6) and explained the NOE for the exocyclic chain of sialic acid (Figure 5) which can only be rationalized in terms of multiple conformers.

The helical properties of GBSP III can be used to rationalize the serological properties of GBSP III. Using fragments of the GBSP III it was ascertained that the epitope had an unusual length dependency, with nonexistent binding for the one repeat unit $[c(de)ba]_1$ and even requiring at least $[c(de)ba]_2$ for suboptimal binding (Wessels et al., 1987b). In addition, the affinity of binding increased with increasing chain length (Wessels et al., 1987a). This observation is consistent with the formation of a unique epitope which exists only in longer oligosaccharides. The driving force for this selectivity is thought to be the reluctance of the immune system to produce antibodies which are associated with short segments of the polysaccharide because of the similarity of the latter to mammalian tissue antigens (Jennings et al., 1984). Although, the model-free analysis of the ^{13}C-relaxation measurements and the molecular dynamic calculations indicated that the polysaccharide is flexible and exists predominantly as a random coil in solution, the local spatial organization of the polymer can be defined by consecutive fragments which have well-defined helical parameters (Perez & Vergelati, 1985; Brisson et al., 1992). As seen from the polar plot of helical parameters obtained from the MD simulation (Figure 3), a wide range of left-handed helices from $n = 2$ ($\rho = -180°$) to $n = 6$ ($\rho = -60°$) are favorable, with the $n = 3$ ($\rho = -120°$) and $\lambda = -0.8$ being the average helix. From the variation of (n, h) as a function (Φ, Ψ) for the 1−6 linkage, a high-order helical region for $n > 5$ occurs over a small range of the (Φ, Ψ) map (Figure 3). Also, a change in ω for the 1−6 linkage would lead to a change in chirality. Hence, the overall topological features of the polysaccharide could change with minor fluctuations in torsion angle about (Φ, Ψ) or ω for the 1−6 linkage (Figure 9), and GBSP III could form extended helices of high order. Such properties would be favorable to the formation of an extended conformation which could easily adapt to an extended binding site. These extended conformations could not be present in short oligosaccharides, since they require multiple repeat units to form ($n > 5$). The gradual displacement of ^{13}C chemical shifts, especially those of GlcNAc, which was observed as the number of repeat units increased for $[c(de)ba]_n$ lends support to the formation of unique conformational features which are length dependent. Hence, the selectivity of the antibodies to GBSP III which are length dependent could be achieved by the recognition of an extended helix made up of multiple repeat units located within the GBSP III random coil. Helices of this type are shown in Figure 9 which could possibly be the source of the epitopes required for binding to GBSP III specific antibodies. Although, there is no direct evidence for this and the precise nature of the conformational epitope cannot be described at this time, there is a precedent because there is strong evidence that the extended epitope associated with the group B menningococcal polysaccharide (α2−8 polysialic acid) is helical (Evans et al., 1995; Brisson et al., 1992).

ACKNOWLEDGMENT

Thanks to Dusan Uhrin for help in the implementation of the NMR pulse sequences, to Wei Zou for preparation of modified GBS III samples, and to R. Somorjai and P. Zhilkin for discussion on minimization strategies for relaxation parameters.

REFERENCES

Acquotti, D., Poppe, L., Dabrowski, J., von der Lieth, C. W., Sonnino, S., & Tettamanti, G. (1990) *J. Am. Chem. Soc. 112*, 7772.

Adams, B., & Lerner, L. (1992) *J. Am. Chem. Soc. 114*, 4827.

Baker, C. J., & Kasper, D. L. (1985) *Rev. Infect. Dis. 7*, 458.

Baker, C. J., & Edwards, M. S. (1988) *Ann. NY Acad. Sci. 459*, 193.
Bax, A., & Davis, D. G. (1985) *J. Magn. Reson. 65*, 355.
Bax, A., Griffey, R. H., & Hawkins, B. L. (1983) *J. Magn. Reson. 55*, 301.
Bax, A., Sklenar, V., Clore, G. M., & Gronenborn, A. M. (1987) *J. Am. Chem. Soc. 109*, 6511.
Bock, K., & Duus, J. O. (1994) *J. Carbohydr. Chem. 13*, 513.
Bock, K., Brignole, A., & Sigurskjold, B. W. (1986) *J. Chem. Soc., Perkin Trans. 2*, 1711.
Bodenhausen, G., & Ruben, D. J. (1980) *Chem. Phys. Lett. 69*, 185.
Bodenhausen, G., Kogler, H., & Ernst, R. R. (1984) *J. Magn. Reson. 58*, 370.
Boyd, J., Hommel, U., & Campbell, I. D. (1990) *Chem. Phys. Lett. 175*, 477.
Breg, J., Kroon-Batenburg, L. M. J., Strecker, G., Montreuil, J., & Vliegenthart, J. F. G. (1989) *Eur. J. Biochem. 178*, 727.
Brisson, J. R., Baumann, H., Imberty, A., Pérez, S., & Jennings, H. A. (1992) *Biochemistry 31*, 4996.
Cooke, R. M., Hale, R. S., Lister, S. G., Shah, G., & Weir, M. P. (1994) *Biochemistry 33*, 10 591.
Cornell, W. D., Cieplak, P., Bayly, C. I., & Kollman, P. A. (1993) *J. Am. Chem. Soc. 115*, 9620.
DiFabio, J. L., Michon, F., Brisson, J. R., Benedi, V. J., Wessels, M. R., Kasper, D. L., & Jennings, H. J. (1989) *Can. J. Chem. 67*, 877.
Evans, S. V., Sigurskjold, B. W., Jennings, H. J., Brisson, J. R., To, R., Tse, W. C., Altman, E., Frosch, M., Weisgerber, C., Kratzin, H. D., Klebert, S., Vaesen, M., Bitter-Suermann, D., Rose, D. R., Young, N. M., & Bundle, D. R. (1995) *Biochemistry 34*, 6737.
Ferrieri, P. (1990) *Rev. Infect. Dis. 12*, S394.
Haasnoot, C. A. G., de Leeuw, F. A. A. M., & Altona, C. (1980) *Tetrahedron 36*, 2783.
Jennings, H. J. (1990) *Curr. Top. Microbiol. Immunol. 150*, 97.
Jennings, H. J., Lugowski, C., & Kasper, D. L. (1981) *Biochemistry 20*, 4511.
Jennings, H. J., Katzenellenbogen, E., Lugowski, C., Michon, F., Roy, R., & Kasper, D. L. (1984) *Pure Appl. Chem. 56*, 893.
Jennings, H. J., Roy, R., & Michon, F. (1985) *J. Immunol. 134*, 2651.
Kay, L. E., Nicholson, L. K., Delaglio, F., Bax, A., & Torchia, D. A. (1992) *J. Magn. Reson. 97*, 359.
Kessler, H., Anders, U., Gemmecker, G., & Steuernagel, S. (1989) *J. Magn. Reson. 85*, 1.
Kogan, G., Uhrin, D., Brisson, J. R., Paoletti, L. C., Kasper, D. L., von Hunolstein, C., Orefici, G., & Jennings, H. J. (1994) *J. Carbohydr. Chem. 13*, 1071.
Kogan, G., Brisson, J. R., Kasper, D. L., von Hunolstein, C., Orefici, G., & Jennings, H. J. (1995) *Carbohydr. Res. 277*, 1.
Kogan, G., Uhrin, D., Brisson, J. R., Paoletti, L. C., Blodgett, A. E., Kasper, D. L., & Jennings, H. J. (1996) *J. Biol. Chem. 271*, 8786.
Leeflang, B. R., & Vliegenthart, J. F. G. (1990) *J. Magn. Reson. 89*, 615.
Lerner, L., & Bax, A. (1986) *J. Magn. Reson. 69*, 375.
Levery, S. B. (1991) *Glycoconjugate J. 8*, 484.
Lipari, G., & Szabo, A. (1980) *Biophys. J. 30*, 489.
Lipari, G., & Szabo, A. (1982a) *J. Am. Chem. Soc. 104*, 4546.
Lipari, G., & Szabo, A. (1982b) *J. Am. Chem. Soc. 104*, 4559.
Marion, D., Ikura, M., & Bax, A. (1989) *J. Magn. Reson. 84*, 425.
Mukhopadhyay, C., Miller, K. E., & Bush, C. A. (1994) *Biopolymers 34*, 21.
Palmer, A. G., III, Rance, M., & Wright, A. (1991) *J. Am. Chem. Soc. 113*, 4371.
Paoletti, L. C., & Johnson, K. D. (1995) *J. Chromatogr. A 705*, 363.
Pearlman, D. A., Case, D. A., Caldwell, J. C., Seibel, G. L., Singh, U. C., Weiner, P., & Kollman, P. A. (1991) AMBER 4.0, University of California, San Francisco.
Perez, S., & Vergelati, C. (1985) *Biopolymers 24*, 1809.
Poppe, L., & van Halbeek, H. (1991) *J. Am. Chem. Soc. 113*, 363.
Poppe, L., Dabrowski, J., von der Lieth, C. W., Numata, M., & Ogawa, T. (1989) *Eur. J. Biochemistry 180*, 337.
Pozsgay, V., Brisson, J. R., & Jennings, H. J. (1990) *Carbohydr. Res. 205*, 133.
Pozsgay, V., Brisson, J. R., & Jennings, H. J. (1991) *J. Org. Chem. 56*, 3377.
Press, W. H., & Teukolsky, S. A. (1991) *Comput. Phys. 5*, 426.
Press, W. H., Flannery, B. P., Teukolsky, S. A., & Vetterling, W. T. (1989) In *Numerical Recipes: The Art of Scientific Computing*, Cambridge University Press, Cambridge.
Rodgers, J. C., & Portoghese, P. S. (1994) *Biopolymers 34*, 1311.
Rutherford, T. J., Jones, C., Davies, D. B., & Elliott, A. C. (1994) *Carbohydr. Res. 265*, 97.
Scarsdale, J. N., Prestegard, J. H., & Yu, R. K. (1990) *Biochemistry 29*, 9843.
Shaka, A. J., & Freeman, R. (1983) *J. Magn. Reson. 51*, 169.
Siebert, H. C., Reuter, G., Schauer, R., von der Lieth, C. W., & Dabrowski, J. (1992) *Biochemistry 31*, 6952.
Sklenar, V., & Bax, A. (1987) *J. Magn. Reson. 74*, 469.
Szyperski, T., Luginbuhl, P., Otting, G., Guntert, P., & Wuthrich, K. (1993) *J. Biomol. NMR 3*, 151.
Tvaroska, I., Hricovini, M., & Petrakova, E. (1989) *Carbohydr. Res. 189*, 359.
Uhrin, D., Mele, A., Boyd, J., Wormald, M. R., & Dwek, R. A. (1992) *J. Magn. Reson. 97*, 411.
Uhrin, D., Brisson, J. R., Kogan, G., & Jennings, H. J. (1994) *J. Magn. Reson., Ser. B 104*, 289.
Uhrin, D., Varma, V., & Brisson, J. R. (1996) *J. Magn. Reson., Ser. A 119*, 120.
van Halbeek, H., & Poppe, L. (1992) *Magn. Reson. Chem. 30*, S74.
Wessels, M. R., & Kasper, D. L. (1989) *J. Exp. Med. 169*, 2121.
Wessels, M. R., Muzoz, A., & Kasper, D. L. (1987a) *Proc. Natl. Acad. Sci. U.S.A. 84*, 9170.
Wessels, M. R., Pozsgay, V., Kasper, D. L., & Jennings, H. J. (1987b) *J. Biol. Chem. 262*, 8262.
Wessels, M. R., DiFabio, J. L., Benedi, V. J., Kasper, D. L., Michon, F., Brisson, J. R., Jelinkova, J., & Jennings, H. J. (1991) *J. Biol. Chem. 266*, 6714.
Woods, R. J., Dwek, R. A., Edge, C. J., & Fraser-Reid, B. (1995) *J. Phys. Chem. 99*, 3832.

BI961819L